Austenite Grain Growth and Precipitate Evolution in a Carburizing Steel with Combined Niobium and Molybdenum Additions

CHARLES M. ENLOE, KIP O. FINDLEY, and JOHN G. SPEER

Austenite grain growth and microalloy precipitate size and composition evolution during thermal processing were investigated in a carburizing steel containing various additions of niobium and molybdenum. Molybdenum delayed the onset of abnormal austenite grain growth and reduced the coarsening of niobium-rich precipitates during isothermal soaking at 1323 K, 1373 K, and 1423 K (1050 °C, 1100 °C, and 1150 °C). Possible mechanisms for the retardation of niobium-rich precipitate coarsening in austenite due to molybdenum are considered. The amount of Nb in solution and in precipitates at 1373 K (1100 °C) did not vary over the holding times evaluated. In contrast, the amount of molybdenum in (Nb,Mo)C precipitates decreased with time, due to rejection of Mo into austenite and/or dissolution of fine Mo-rich precipitates. In hot-rolled alloys, soaking in the austenite regime resulted in coarsening of the niobium-rich precipitates at a rate that exceeded that predicted by the Lifshitz-Slyozov-Wagner relation for volume-diffusion-controlled coarsening. This behavior is attributed to an initial bimodal precipitate size distribution in hot-rolled alloys that results in accelerated coarsening rates during soaking. Modification of the initial precipitate size distribution by thermal processing significantly lowered precipitate coarsening rates during soaking and delayed the associated onset of abnormal austenite grain growth.

DOI: 10.1007/s11661-015-3103-1

I. INTRODUCTION & BACKGROUND

MICROALLOY additions are increasingly employed for the control of microstructure to achieve desired properties in automotive, structural, and engineering steels. In manufacturing processes that require reheating, *e.g.*, slab and ingot reheating after casting and high-temperature carburizing, the effect of microalloying additions such as niobium (Nb) and titanium (Ti) on austenite grain size at elevated temperatures is of importance as abnormal coarsening of the austenite grain structure can result in the general degradation of fatigue performance and toughness.[1] The coarsening of microalloy precipitates in austenite is thought to be the controlling factor in the onset of abnormal grain growth, and solute drag is assumed to be of secondary significance.[2–4] Thus, microalloyed steel variants have been developed which employ fine Nb- and/or Ti–rich carbonitrides to suppress grain growth and provide resistance to austenite grain coarsening.[2,4–9] This study investigates the effectiveness of both molybdenum (Mo) additions and thermal processing to increase the coarsening resistance of Nb-rich precipitate distributions in austenite and delay the associated onset of abnormal grain growth.

A. *Grain Refinement with Microalloy Additions*

The mechanism of grain boundary pinning was first quantified by Zener with the classic expression shown in Eq. [1][3]

$$R = \xi \cdot \left(\frac{r}{f}\right), \qquad [1]$$

where R is the average radius of a shrinking grain pinned by a two-dimensional precipitate array of volume fraction, f, and average radius, r. Equation [1] demonstrates that austenite grain size can be stabilized by second phase precipitates when the volume fraction of precipitates is sufficiently high and their size sufficiently small. In Zener's model $\xi = 4/3$, but more sophisticated derivations incorporating grain size uniformity have produced the pre-factor relation shown in Eq. [2].[3]

$$\xi = \frac{\pi}{6}\left(\frac{3}{2} - \frac{2}{Z}\right) \qquad [2]$$

The size advantage parameter, Z, a measure of grain size uniformity, is defined as the ratio of the largest grain radius to average grain radius and typically ranges from $Z = \sqrt{2}$ to $Z = 2$. Equations [1] and [2] demonstrate

CHARLES M. ENLOE, Materials Engineer, is with General Motors LLC, GM Product Development«Materials Engineering, Warren, MI 48090. Contact e-mail: charles.enloe@gm.com KIP O. FINDLEY, Associate Professor, and JOHN G. SPEER, John Henry Moore Distinguished Professor, Director, are with the George S. Ansell Department of Metallurgical and Materials Engineering, Advanced Steel Processing and Products Research Center, Colorado School of Mines, Golden, CO 80401.

Manuscript submitted January 16, 2015.
Article published online August 27, 2015

that greater grain size uniformity is desirable for resistance to the onset of abnormal grain growth at a given r/f value. The r/f value is a time-dependent function of the precipitate size distribution evolution, and abnormal grain coarsening resistance is, therefore, believed to be limited by the coarsening of the precipitates (increasing r) at elevated temperature. Further alloy and processing developments to enhance microalloy precipitate coarsening resistance would be beneficial for engineering applications.

Microalloy precipitate coarsening during isothermal soaking has been shown in previous studies to follow the Lifshitz-Slyozov-Wagner (LSW) relation for long range volume-diffusion-controlled coarsening shown in Eq. [3][10–12]:

$$r^3 - r_0^3 = \frac{8 D_M \Omega [M] \gamma_{P/M}}{9RT} \cdot t, \qquad [3]$$

where r and r_0 are the instantaneous average and initial average precipitate radii, respectively, D_M is the diffusion coefficient for the precipitate forming element (rate controlling species) in the given matrix, $[M]$ is the concentration in solution of the precipitate forming element (rate controlling species) in atomic fraction, Ω is the molar volume of the precipitate, $\gamma_{P/M}$ is the precipitate/matrix interfacial energy, R is the ideal gas constant, T is absolute temperature, and t is the time in seconds. The LSW expression predicts that coarsening precipitates will adopt a time-independent and self-consistent size distribution with a limiting precipitate size of $r_{max} = 3r/2$.[10] The LSW expression also predicts that a reduction in the coarsening rate of microalloy precipitates in austenite may be achieved through a reduction in D_M, $[M]$, or $\gamma_{P/M}$, and specific alloying additions such as Mo may affect these parameters as reported in previous studies.[13–16] The assumption of isothermal coarsening in the LSW model, however, may not be valid in many industrial applications where thermo-mechanical processes are highly variable. Therefore, one may expect the LSW expression to be an inadequate predictor, for example, of average precipitate radius evolution during reheating and soaking of hot-rolled steels.

B. *Microalloy Precipitate Behavior*

Titanium and niobium are among the common alloying additions in modern, grain-refined steels. Titanium nitride (TiN) has been characterized as the most effective grain growth inhibiting microalloy precipitate at temperatures above 1323 K (1050 °C) by direct comparison to additions of Nb, V, or Al.[2] This assertion assumes comparable microalloy concentrations and average precipitate size and is a consequence of the greater volume fraction provided by the lower solubility of TiN in austenite relative to other microalloy carbides and nitrides. High-temperature precipitation of TiN, however, can also be detrimental to its grain refining capabilities due to precipitate growth and coarsening at elevated temperatures.

Relative to Ti, Nb displays moderate solubility as both a nitride and a carbide. The nitride form of the microalloy precipitate is more stable than the carbide, but alloying (including high C/N ratios and additions of Ti) of steels for high-temperature stability limits the amount of free N. The two forms, NbC and NbN, are mutually soluble, and the carbonitride Nb(C,N) is both an effective grain refiner in high-temperature processing with additions up to 0.10 wt pct Nb and is useful in retarding the onset of recrystallization during hot deformation in appropriate temperature regimes.[17–21] The Nb-rich precipitate size distribution can be highly influenced by thermo-mechanical history, and the greater solubility of Nb-rich precipitates relative to TiN often results in finer precipitate distributions and subsequent grain refining behavior.[6–8,19,22–24]

The mixed carbonitride precipitate (Nb,Ti)(C,N) and its components have also been the subject of study.[25–32] Titanium incorporation into (Nb,Ti)(C,N) precipitates is reported to improve the elevated temperature stability relative to Nb(C,N). That is, Ti and Nb are reported to exhibit complementary effects as components in a mixed carbonitride, whereby Ti reduces high-temperature solubility, and Nb(C,N) provides larger attainable volume fractions of fine carbonitrides at low temperature.[2,31,33,34]

C. *The Effect of Mo on Microalloy Precipitation*

Molybdenum is traditionally added to low alloy steels for hardenability. Studies suggest, however, that Mo affects the precipitate size distribution evolution through various mechanisms and, therefore, may affect associated grain growth.[14,35–37]

Previous investigations report that additions of Mn, Mo, and V to a Nb-microalloyed steel all act to reduce the dynamic precipitation of Nb(C,N) during hot compression in the temperature range 1148 K to 1423 K (875 °C to 1150 °C).[13,38,39] It has been speculated that both Mo and Mn act to lower the diffusivity of Nb in austenite through a reduction in the frequency factor of the diffusion coefficient but not through an increase of the diffusion activation energy.[14,15] In ferrite, Mo is reported to both segregate to the precipitate-matrix interface and to slow the diffusion of Nb to the carbonitride, thus reducing the coarsening rate.[40–42] Segregation of Mo to the precipitate-prior austenite interface was not observed in a recent investigation, however, following austenitic soaking of Mo-bearing, Nb-microalloyed steel.[43] Numerous studies report significant Mo incorporation as MoC in microalloy carbonitrides (up to 40 wt pct) in Nb-microalloyed low alloy steel with various thermo-mechanical histories.[13,14,16,25,41,43–48]

A greater amount of study to date has focused on the effect of Mo on the evolution of Ti-rich precipitates in ferrite.[49–55] The various effects of Mo on Ti-rich precipitate development in ferrite are of interest to the current study as a similar mechanism may be operable for Nb-rich precipitates in ferrite and/or austenite. The effect of Mo on the formation of an increased number of

fine (less than 10 nm), coarsening resistant (Ti,Mo)C precipitates during slow cooling and/or reheating is attributed by Chen *et al.* to the increased number of precipitate nucleation sites due to the refinement of bainitic ferrite by Mo.[53] Jang *et al.* employed first-principles calculations to suggest that incorporation of Mo into the ternary carbide, (Ti,Mo)C, results in a reduction in the lattice mismatch between the precipitate and the matrix and associated decreases in the barrier to nucleation in ferrite and precipitate/matrix interfacial energy; there is also an associated decrease in solute Ti.[54]

To further utilize the coarsening resistance effects of Mo in industrial processes, the mechanisms by which Mo affects precipitate composition and size evolution require further definition. The intent of this investigation, as outlined in the following methodology, was to quantify and elucidate the effect of Mo additions and thermal processing on precipitate and grain size evolution. Particular focus was placed on the effect of Mo on the onset of abnormal grain growth in Nb-microalloyed austenite.

II. EXPERIMENTAL METHODOLOGY

The effects of Nb, Mo, and thermal history on grain size evolution, precipitate size distribution (PSD), and composition evolution were investigated using light optical microscopy, electrochemical dissolution, and precipitate extraction in conjunction with inductively coupled plasma mass spectroscopy (ICP-MS), and transmission electron microscopy (TEM).

A. *Materials*

Four experimental alloy compositions, as measured by optical emission spectroscopy, are shown in Table I. The base steel composition, SAE 4120, was selected for its industrial relevance as a commonly used carburizing alloy, and experimental alloys were derived from the base composition to investigate the effects of Mo and various levels of Nb addition on precipitate and grain coarsening. Previous studies show that hypo-stoichiometric Ti additions (with respect to N) yield the smallest and most coarsening resistant TiN precipitates prior to precipitation of complex Nb-bearing precipitates during the steelmaking process.[56] Thus, a target Ti/N weight fraction of 1.25, which falls below the stoichiometric ratio of 3.42, was specified for each experimental alloy.

Two distinct target Nb and Mo additions were chosen (Nb: 0.05 and 0.10 wt pct; Mo: 0.0 and 0.30 wt pct) to assess the combined effects of Nb and Mo. An increased Mo addition relative to standard SAE 4120 was chosen to enhance the effects of Mo on microstructure and precipitate evolution. The experimental alloys are designated as LNb (low Nb addition), HNb (high Nb addition), MoLNb (Mo and low Nb addition), and MoHNb (Mo and high Nb addition) as shown in Table I below.

Following vacuum induction melting and casting, the ingots were reheated to 1523 K (1250 °C), upset forged and cropped to the appropriate billet geometry for subsequent hot-rolling, and then air-cooled. These billets, 69.9 mm (2.75 in) thick, were then reheated at 1523 K (1250 °C) for 240 minutes and rolled at per pass reductions of 3.175 mm (0.125 in) to 6.35 mm (0.25 in) to achieve a final thickness of 10.16 mm (0.4 in) at a finishing temperature of 1373 K (1100 °C).

To assess the microalloy precipitation behavior during hot-rolling, the amount of solute Nb as a function of temperature was estimated with the solubility product of Narita[57] for NbC. Figure 1 shows solubility isotherms for NbC at temperatures of 1173 K, 1373 K, and 1523 K (900 °C, 1100 °C, and 1250 °C). Solutionizing treatments at 1523 K (1250 °C) are expected to be insufficient for dissolution of all NbC precipitates for 0.2 wt pct C alloys with Nb additions greater than 0.086 wt pct. Full NbC dissolution is, however, expected in the low Nb alloys containing nominal additions of 0.05 wt pct Nb. The calculated equilibrium amounts of solute Nb and Nb precipitated as NbC are shown graphically in Figure 1 at the finishing temperature of 1373 K (1100 °C) for the low (0.05 wt pct) and high Nb (0.11 wt pct) concentrations, respectively. The amount of solute Nb is 0.023 and 0.025 wt pct for the low and high Nb conditions, respectively, while the amount of Nb precipitated as NbC is 0.027 and 0.085 wt pct for the low and high Nb conditions, respectively.

B. *Thermal Processing*

To determine the effect of Mo and thermal processing on grain and precipitate size evolution at elevated temperature, the hot-rolled experimental alloys were processed according to the schedules shown in Figures 2(a) through (d). The thermal treatments shown in Figures 2(a) through (c) were conducted in a laboratory box furnace using 1 cm^3 specimens, which were immediately water quenched (identified as *WQ*) following removal from the furnace. The thermal treatment shown in Figure 2(d) was conducted using a Gleeble® 3500. Each thermal processing sequence accomplished a different objective:

1. To assess the effect of Mo on grain growth and precipitate evolution in hot-rolled alloys, specimens

Table I. Chemical Composition of SAE 4120 Modified Alloys (Weight Percent)

Wt Pct	C	Mn	Si	Ni	Cr	Mo	Ti	Nb	V	Al	N	S	P	Ti/N
LNb	0.21	0.89	0.16	—	0.50	0.00	0.015	0.044	—	0.025	0.0083	0.013	0.007	1.8
HNb	0.21	0.83	0.15	—	0.49	0.01	0.012	0.104	—	0.022	0.0090	0.013	0.007	1.3
MoLNb	0.21	0.86	0.15	—	0.50	0.29	0.013	0.043	—	0.024	0.0078	0.014	0.007	1.7
MoHNb	0.21	0.86	0.15	—	0.50	0.30	0.015	0.118	—	0.021	0.0082	0.016	0.007	1.8

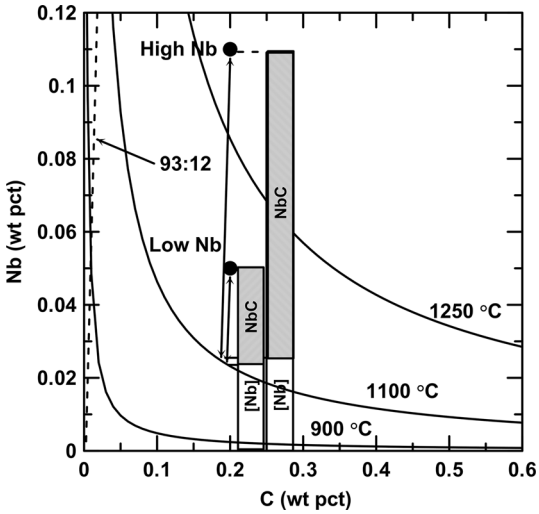

Fig. 1—Solubility product isotherms for NbC in austenite at 1173 K, 1373 K, and 1523 K (900 °C, 1100 °C, and 1250 °C). The approximate chemistries of the low and high Nb alloys are shown to illustrate the solubility of NbC at various processing temperatures. The dashed stoichiometric line (93:12) for NbC is shown in addition to predicted equilibrium amounts of solute Nb, labeled *[Nb]*, and Nb in NbC, labeled *NbC*, for both alloy chemistries at a finish rolling temperature of 1373 K (1100 °C).

of the four experimental alloys were reheated at a constant heating rate of 10 °C/min to soaking temperatures of 1323 K or 1373 K (1050 °C or 1100 °C) for 0, 30, 60, and 90 minutes, and 0, 6, 30, 60, and 90 minutes, respectively, and water quenched (Figure 2(a)).

2. To assess the effect of Mo on Nb-rich precipitate evolution in ferrite and associated secondary hardening behavior of hot-rolled alloys, specimens of the four experimental alloys were tempered at temperatures of 723 K, 773 K, 823 K, 873 K, 923 K, or 973 K (450 °C, 500 °C, 550 °C, 600 °C, 650 °C, or 700 °C) for 120 minutes and water quenched (Figure 2(b)).
3. To assess the effect of tempering prior to reheating on subsequent grain growth and precipitate evolution, specimens of the four experimental alloys were tempered at 873 K (600 °C) for 120 minutes prior to reheating and soaking at 1373 K (1100 °C) for 60 minutes and 1323 K (1050 °C) for 90 minutes (Figure 2(c)). The tempering pre-treatment was selected to coincide with peak secondary hardening of Mo-bearing specimens, a condition indicative of an increased volume fraction of fine precipitates relative to the hot-rolled condition as discussed in Section III–B.
4. A Gleeble® 3500 was used to assess the precipitate coarsening resistance in the absence of an initial distribution of Nb-rich precipitates. Samples of the MoLNb and LNb alloys were held at 1523 K (1250 °C) for 10 minutes to solutionize all Nb-bearing precipitates and helium (He) quenched to room temperature (at a rate of approximately 250 K/s) to ensure that Nb remained in solution. The samples were then reheated to 1323 K, 1373 K, or 1423 K (1050 °C, 1100 °C, or 1150 °C) and held for 0, 30, and 60 minutes prior to a final He quench (Figure 2(d)).

C. *Metallography*

Metallographic specimens were prepared using standard techniques, and hot-rolled specimens were etched with 2 vol pct nital. Specimens processed according to Figures 2(a) and (c) were etched to reveal prior austenite grain boundaries for grain growth studies using a saturated aqueous picric acid solution containing 1 vol pct HCl and 1 vol pct Teepol surfactant at 338 K (65 °C). Selected specimens processed according to Figure 2(d) (MoLNb alloy, reheated to 1373 K (1100 °C) for 0-60 minutes) were also etched to reveal prior austenite grains. Prior austenite grain size was analyzed by determining the mean lineal intercept (MLI) and lineal intercept distribution with the aid of image analysis software. A minimum of 600 intercepts were counted for each tested condition from a minimum of 10 randomly chosen fields of view.

D. *Electron Microscopy*

Carbon extraction replicas of both hot-rolled samples and samples processed according to Figures 2(a), (c), and (d) were prepared by physical vapor deposition of a thin carbon film on metallographic specimens following etching with 2 vol pct nital. Carbon films were lifted from the metallic sample using an aqueous solution containing 3.3 vol pct nitric acid, 3.3 vol pct acetic acid, and 0.1 vol pct hydrofluoric acid at room temperature, rinsed in a solution containing 10 vol pct deionized water in methanol, and collected on 200 mesh Cu grids for subsequent TEM analyses. Precipitate size distribution analyses were conducted on bright-field TEM micrographs of carbon extraction replicas like the example micrograph shown in Figure 3. Representative precipitate morphologies are identified in Figure 3 in addition to artifacts commonly observed during TEM analyses, *i.e.*, contrast not arising from extracted particles. The majority of the precipitates could be classified into one of three categories: cuboidal TiN precipitates, spheroidal Nb-rich precipitates, and precipitates containing both Nb and Ti with a mixed cuboidal and spheroidal morphology. The sizes of cuboidal and mixed morphology precipitates were measured as the average length of their long and short axes, and spheroidal precipitates were measured by their diameter as illustrated. A minimum of 300 precipitates were measured for each specimen condition from a minimum of two carbon extraction replicas and 10 randomly chosen fields of view. Care was taken that contrast artifacts from the specimen preparation process were not interpreted as precipitates and counted as such. Annular dark-field scanning TEM was employed to confirm that sample preparation artifacts were not responsible for the apparent presence of very small (diameters less than 10 nm) precipitates in selected bright-field TEM images.

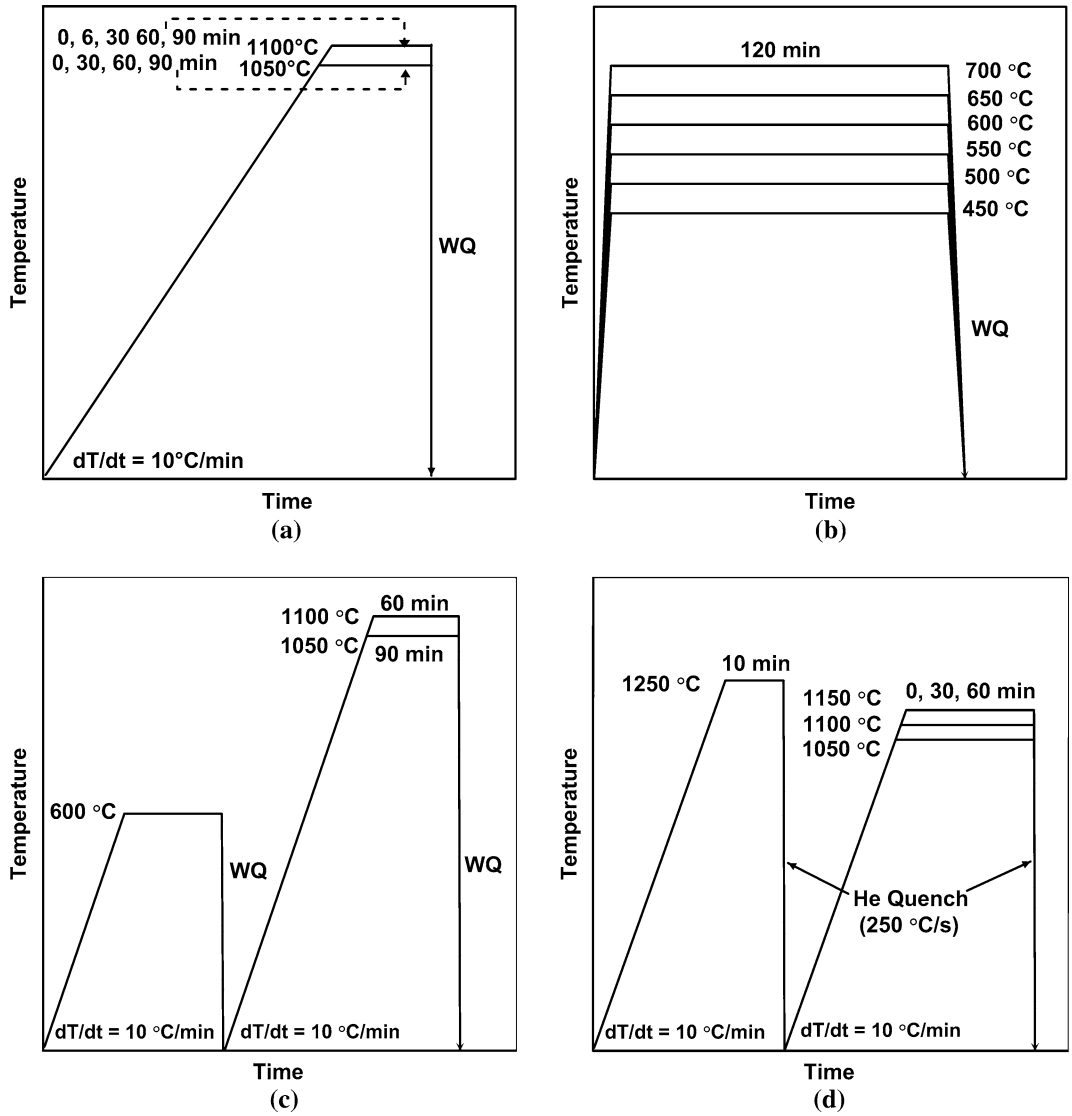

Fig. 2—Thermal schedules of hot-rolled alloys for analysis of microalloy precipitate and microstructural evolution during (*a*) soaking at elevated temperature, (*b*) ferrite tempering, (*c*) tempering followed by soaking at elevated temperature, and (*d*) solutionizing followed by soaking at elevated temperature.

E. *Thermo-kinetic Modeling*

As a supplement to experimental results, MatCalc© was employed to model the effects of a pre-existing precipitate distribution in a hot-rolled alloy on the average precipitate radius evolution during reheating and soaking in austenite. A model HNb alloy (Fe-0.20 C-0.10 Nb-0.015 Ti-0.009 N wt pct) was employed with two different precipitate distribution conditions prior to reheating. Firstly, a bimodal precipitate distribution was developed by simulating soaking at 1523 K (1250 °C) for 120 minutes followed by a slow quench (2 K/s) to room temperature. This condition was then reheated to 1373 K (1100 °C) at 10 K/min, and the average precipitate radius was compared to a condition in which no prior distribution was developed prior to reheating. Precipitate nucleation was allowed on grain boundaries, subgrain boundaries, and dislocations in both austenite and ferrite. Because four phase coexistence, *i.e.*, ferrite, austenite, cementite, and the carbonitride phase, is precluded in the MatCalc© software, it was necessary to approximate matrix phase transformation temperatures during thermal processing simulations to a single value. The austenite to ferrite transformation temperature during cooling was approximated as 973 K (700 °C), and the ferrite to austenite transformation temperature during reheating was approximated as 1073 K (800 °C). The thermodynamic and diffusion databases used were *mc_steel.tdb* and *mc_sample_fe.ddb*, respectively. Additional pertinent model assumptions and parameter values are listed in Table II, where $\gamma_{P/M}$ is the precipitate-matrix surface energy, ρ is the dislocation density, D is the grain diameter, E is the Young's modulus, N is the number of precipitate classes, m is the matrix diffusion enhancement factor, and n is the nucleation constant.

F. *Electrochemical Dissolution and Precipitate Extraction*

To determine the effect of Mo on Nb solubility and precipitate composition in the hot-rolled alloys, both prior to reheating and during holding at austenitic temperatures, electrochemical dissolution, and precipitate extraction were performed using a procedure outlined by Rothleutner[58] after Kurosawa *et al.*[59] Two specimens per hot-rolled alloy and two specimens per alloy soaked at 1373 K (1100 °C) for 0, 30, and 60 minutes were analyzed by inductively coupled plasma mass spectrometry (ICP-MS). The detection limits of the ICP-MS analyses for Mo and Nb are 0.3 parts per billion or better (by weight). All chemicals used in this technique were ACS (American Chemical Society) reagent grade or better.

III. RESULTS & DISCUSSION

A. *Microstructure Analyses*

Figure 4 shows representative light optical micrographs for LNb and MoLNb alloys in the hot-rolled condition. Hot-rolled microstructures of the Mo-free alloys, LNb and HNb, consist of polygonal ferrite and pearlite as shown for the LNb alloy in Figure 4(a). The Mo-containing alloys display a refined, lath-type ferrite morphology as shown for the MoLNb alloy in Figure 4(b).

Figures 5(a) through (d) show representative prior austenite grain structures of the experimental alloys after soaking for 60 minutes at 1373 K (1100 °C) and water quenching. Figure 5(e) is included for comparison and shows the equiaxed prior austenite grain structure of the MoHNb alloy reheated to 1373 K (1100 °C) and water quenched without isothermal holding. Figures 5(a) and (c) show that significant abnormal grain growth (AGG) occurs in the LNb and MoLNb alloys, respectively, and qualitatively there is a slight reduction of AGG due to a Mo addition in the MoLNb alloy relative to the LNb alloy. Higher Nb levels in the HNb and MoHNb alloys have a more pronounced effect on reducing AGG as shown in Figures 5(b) and (d). These effects of Mo and Nb were consistent throughout all alloy-process combinations that were studied. The onset of AGG was observed, however, in all hot-rolled experimental alloys during soaking at 1373 K (1100 °C) for 60 minutes.

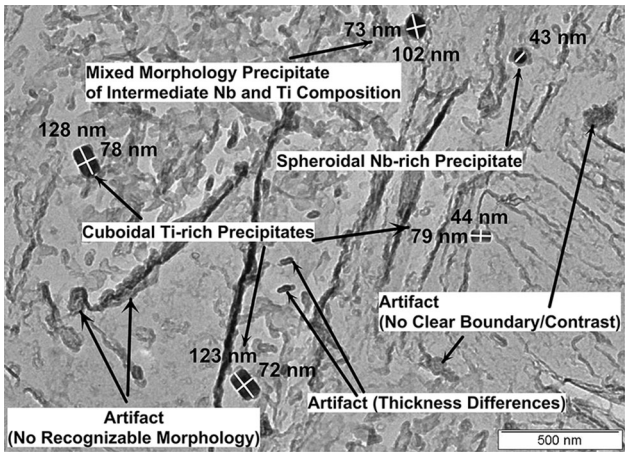

Fig. 3—Example TEM micrograph of a carbon extraction replica illustrating the measurement technique for cuboidal and spheroidal precipitates from a MoLNb sample reheated to 1373 K (1100 °C), held for 60 min and water quenched.

To quantify the effects of Nb and Mo in mitigating austenite AGG, mean lineal intercept lengths for prior austenite grain structures of selected alloy conditions processed according to Figures 2(a), (c), and (d) were determined and are shown in Figure 6 as a function of square root of holding time. Samples tempered prior to soaking are identified as *600T* in Figures 6(c) and (d), and solutionized MoLNb samples subsequently soaked at 1373 K (1100 °C) are identified as *solutionized* in Figure 6(d). Normal grain growth processes exhibit root time dependencies,[3] and Figure 6 is constructed to highlight variation from this behavior. Here, the onset of AGG is defined by the presence of one or more prior austenite grains with measured diameters greater than three times the average measured grain diameter using the approximation of average grain diameter as 1.61·MLI.[4] For clarity of subsequent discussion, grain size, and MLI will be referenced interchangeably. As shown, the LNb alloy exhibited the greatest amount of grain growth and also demonstrated the greatest amount of AGG, whereas the Mo additions in the MoLNb and MoHNb alloys act to lower the average grain size significantly at extended holding times at 1323 K (1050 °C) (Figure 7(a)) and 1373 K (1100 °C) (Figure 6(b)). Figures 6(a) and (b) also clearly show that the high Nb alloys (HNb and MoHNb) are much more capable of retarding the onset of abnormal growth when compared to the low Nb alloys (LNb and MoLNb). The grain refinement effects of both Mo and Nb become more pronounced with soaking time and temperature as illustrated by comparison of Figures 6(a) and (b).

As shown in Figure 2(a), some specimens were reheated to 1373 K (1100 °C) and immediately water quenched to assess the austenite grain size distribution at the onset of soaking. The standard deviation of lineal intercept length, a convenient approximation of the grain size distribution non-uniformity, and relative

Table II. Parameters Used for Calculation of Average Precipitate Radius Evolution

	$\gamma_{P/M}$ (J/m^2)	ρ (m^{-2})	D (μm)	$E/10^6$ (Pa)	N	m	n
Ferrite	0.8	1×10^{14}	20	210000-75·T (°C)	50	1	1
Austenite	0.8	1×10^{12}	50	193000-73.333·T (°C)	50	1	1

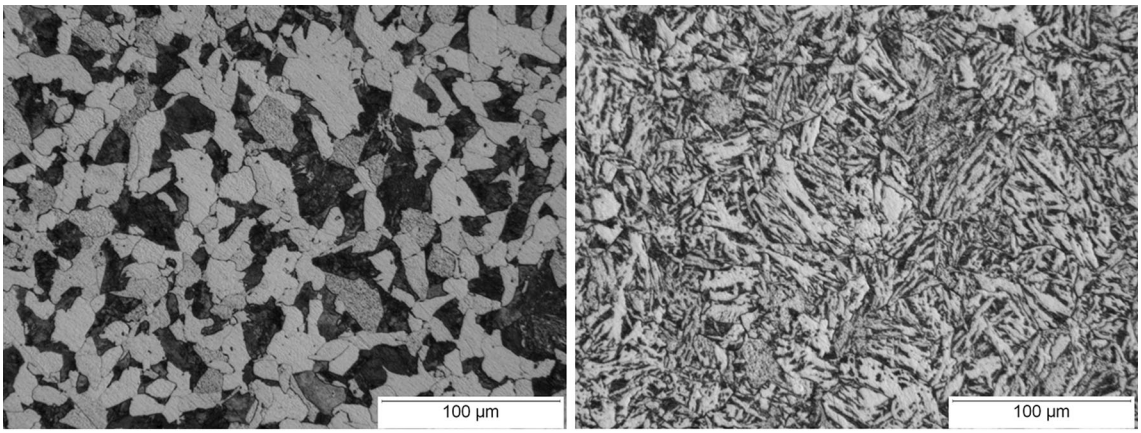

Fig. 4—Representative light optical micrographs of (*a*) hot-rolled LNb and (*b*) hot-rolled MoLNb-etched with 2 vol pct Nital.

estimate of the size advantage parameter, Z, in Eq. [2], was calculated for each specimen reheated to 1373 K (1100 °C) and water quenched. The calculated standard deviations are shown in Table III along with calculated mean lineal intercept lengths and the ratios of standard deviation to mean lineal intercept length. As a measure of grain size distribution non-uniformity, it may be considered that the ratio of the standard deviation of the distribution to the mean of the distribution is related to the capillary driving force for grain growth. This is because the expected maximum grain size in a given volume increases relative to the mean grain size as the standard deviation to mean ratio increases.[3] The Mo-containing alloys exhibit greater grain size uniformity relative to those of the Mo-free alloys. Therefore, the capillary driving force for the onset of abnormal growth during further soaking is greater in Mo-free alloys relative to Mo-containing alloys.

Figure 6 also highlights the effect of tempering to achieve peak secondary hardening of hot-rolled alloys, indicative of an increased volume fraction of fine precipitates, prior to reheating to elevated temperatures. Tempering at 873 K (600 °C) for 120 minutes prior to holding for 90 minutes at 1323 K (1050 °C) both greatly reduces the measured austenite grain size and prevents the onset of AGG in all experimental alloys soaked at 1323 K (1050 °C) (Figure 6(c)). Tempering also lowers the austenite grain size for samples held at 1373 K (1100 °C) for 60 minutes, but AGG is observed for this condition in all alloys as noted in Figure 6(d).

Like tempering, solutionizing of MoLNb at 1523 K (1250 °C) for 10 minutes and quenching prior to soaking at 1373 K (1100 °C) for 60 minutes reduces the measured austenite grain size relative to the hot-rolled and soaked condition as shown in Figure 6(d); in addition, AGG is not present. Table IV lists the mean lineal intercept lengths of both solutionized and tempered samples shown in Figure 6 for clarity. A hypothesis for the observed grain refinement due to thermal processing prior to soaking will be discussed in a subsequent section.

B. *Secondary Hardening Analysis*

Figure 7 illustrates the Vickers hardness measurements of hot-rolled specimens of each experimental alloy tempered according to Figure 2(b). Secondary hardening of the hot-rolled, Mo-containing alloys is present following tempering for 120 minutes at 873 K to 898 K (600 °C to 625 °C). However, a distinct secondary hardening peak is absent in the hot-rolled, Mo-free alloys, and hardness reaches a maximum at temperatures less than 873 K (600 °C). Molybdenum additions, therefore, result in an increase in the magnitude of the secondary hardening response at increased tempering temperatures. In the absence of a more potent carbide former such as Nb, previous studies have shown that Mo- and Cr-bearing alloys exhibit resistance to temper softening and secondary hardening by precipitation of Mo- and Cr-rich carbides in the temperature range of interest, and Mo is the more potent of the two additions.[60–62] However, neither Mo_2C nor any additional alloy carbide, *e.g.*, Cr_7C_3, was observed during TEM investigations of tempered specimens. This observation is in agreement with previously reported studies by Kanazawa *et al.* for Nb, Mo-bearing steels.[46] In these alloys, Mo_2C precipitates are not the cause for increased secondary hardening. Because recent investigations[54] suggest that Mo lowers the interfacial energy of (Ti,Mo)C in ferrite through substitution on the metallic sublattice, and a similar mechanism that favors nucleation may be operable for (Nb,Mo)C in ferrite, the increase in secondary hardening may be attributable to an increase in the number of newly nucleated Nb-rich precipitates during tempering due to Mo additions. Alternatively, this behavior may be due to an increased number of precipitate nucleation sites associated with refinement of the hot-rolled microstructure by Mo. The Mo-containing alloys have an increased temperature to attain the peak hardness relative to the alloys that do not contain Mo, which is attributed to the possible retarding effect of Mo on Nb-rich precipitate coarsening kinetics in ferrite.

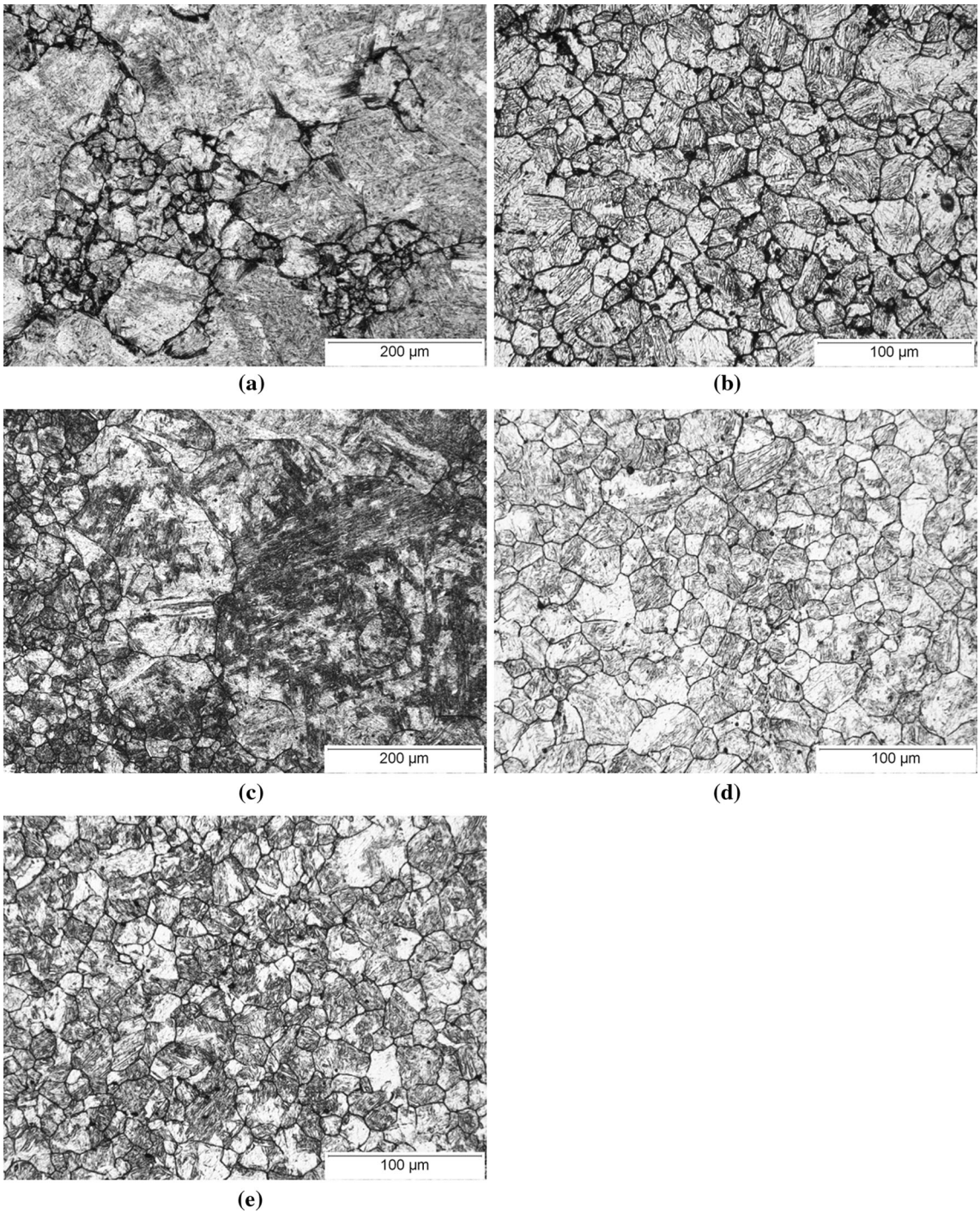

Fig. 5—Representative light optical micrographs showing the prior austenite grain structure of hot-rolled (*a*) LNb, (*b*) HNb, (*c*) MoLNb, and (*d*) MoHNb soaked at 1373 K (1100 °C) for 60 min prior to water quenching. For comparison, hot-rolled MoHNb reheated to 1373 K (1100 °C) and held for 0 min prior to water quench is shown in (*e*) -etched by immersion in saturated aqueous picric acid containing 1 vol pct HCl and 1 vol pct Teepol surfactant at 338 K (65 °C). Note differences in scale bars.

C. *Precipitate Size Distribution Analyses*

The precipitate size distribution (PSD) evolution was investigated in light of the effects of variations in Mo and Nb content and thermal history on grain growth behavior in austenite. Representative micrographs of carbon extraction replicas are shown in Figure 8 for hot-rolled MoLNb soaked at 1373 K (1100 °C) for times between 0 and 60 minutes. Figure 8 qualitatively illustrates the increase in average precipitate size during holding at elevated temperature, and example spheroidal, mixed morphology, and cuboidal precipitates are identified. From the measured distributions, the

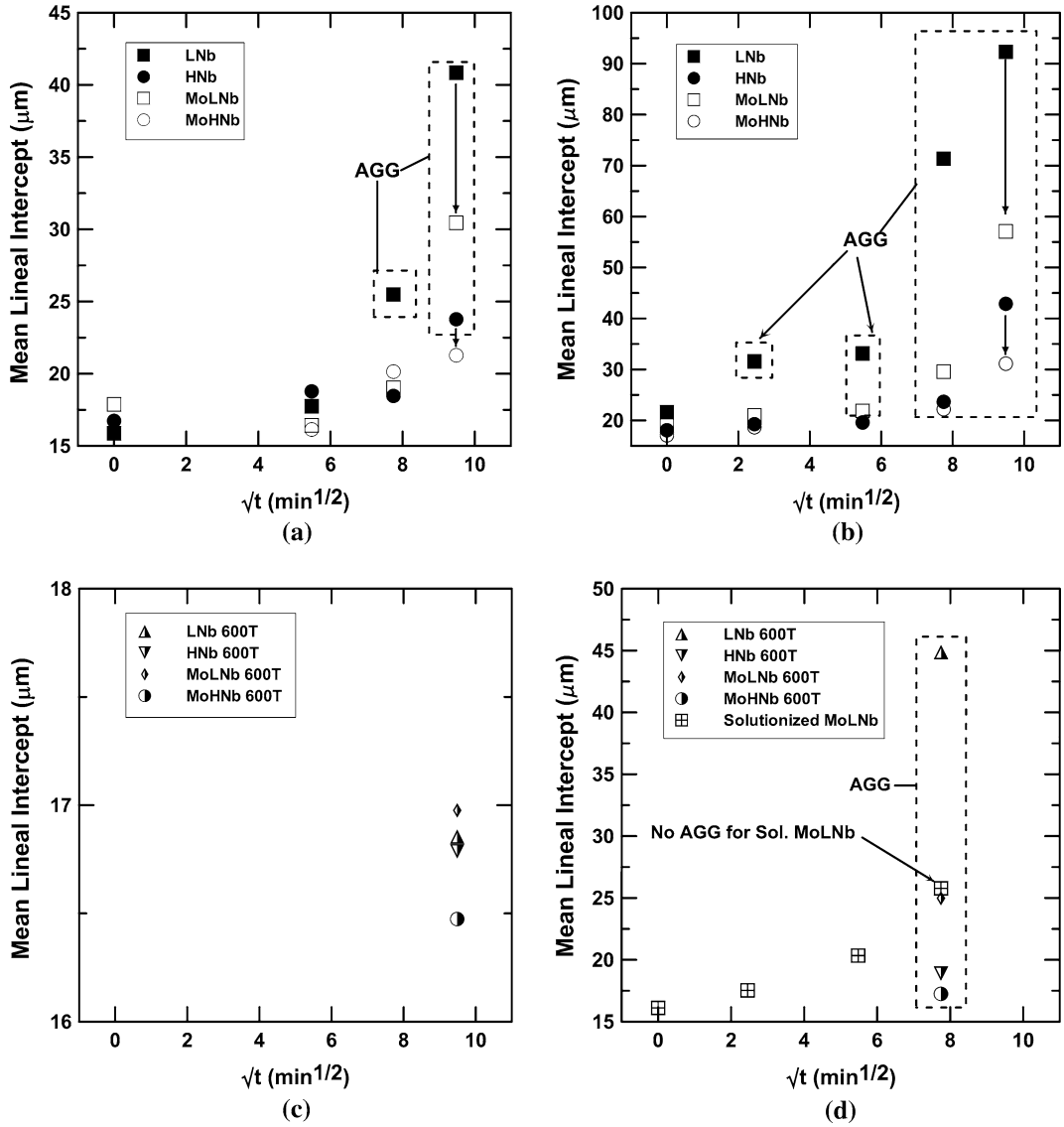

Fig. 6—Mean lineal intercept (MLI) of prior austenite grain structures as a function of the square root of holding time for experimental hot-rolled alloys at (*a*) 1323 K (1050 °C) and (*b*) 1373 K (1100 °C). Tempered (identified as *600T*) and solutionized MoLNb conditions are shown separately in (*c*) 1323 K (1050 °C) and (*d*) 1373 K (1100 °C) for clarity. Samples exhibiting abnormal grain growth (AGG) are identified. Vertical arrows in (a) and (b) indicate the reduction of MLI at the longest holding times at each respective temperature due to the Mo addition. A minimum of 600 intercepts were counted for each condition. Errors of ±0.79 μm for each datum are estimated from a measurement error of ±4 pixels for each intercept length. Note differences in vertical axes.

evolution of the average precipitate radius, r, was determined and compared between conditions and to the coarsening rates $\left(\frac{d(r^3)}{dt}\right)$ predicted by the LSW equation. Figure 9 shows the cube of the average precipitate radius as a function of holding time, t, at 1323 K, 1373 K, and 1423 K (1050 °C, 1100 °C, and 1150 °C) for previously hot-rolled, tempered (identified as *600T*), and solutionized specimens (identified as *solutionized*). Coarsening rates are defined as the average slope of the r^3 *vs* t data. The alloys containing Mo exhibit a significant decrease in precipitate radius and coarsening rate in all tested conditions compared to the Mo-free alloys as indicated by arrows. In contrast, an increase in Nb concentration increases the precipitate coarsening rate. Either solutionizing or tempering for 120 minutes at 873 K (600 °C) prior to reheating and soaking at elevated temperature results in significantly reduced precipitate radii for the tested range of soaking temperatures and times.

The observed coarsening rates of the hot-rolled alloys and solutionized alloys were compared to rates predicted by the LSW model shown in Eq. [3] for NbC with parameters obtained from literature (Table V). The NbC solubility and the Nb diffusion coefficient were calculated at the specified temperatures using values of Narita[57] and Gladman,[3] respectively. The ratios of the observed coarsening rates, as defined by the average slopes of the r^3 *vs* t curves, to the predicted rates of the LSW equation at various temperatures are shown in

Table VI. The rates (slopes) predicted by the LSW equation are shown as dashed lines in Figure 9. The observed coarsening rates of the hot-rolled alloys are much greater than those predicted by the LSW model. The results also show that the addition of 0.3 wt pct Mo to the experimental alloys reduces the precipitate coarsening rate by 12-13 pct at 1323 K (1050 °C) and by 55-61 pct at 1373 K (1100 °C). The HNb conditions have slightly higher amounts of solute Nb compared to the LNb conditions, which should slightly increase the precipitate coarsening rate (see calculations by L'Ecuyer *et al.*[39]). However, a 95-97 pct increase and 219-270 pct increase in precipitate coarsening rates are observed in the high Nb conditions compared to the low Nb conditions at 1323 K and 1373 K (1050 °C and 1100 °C), respectively.

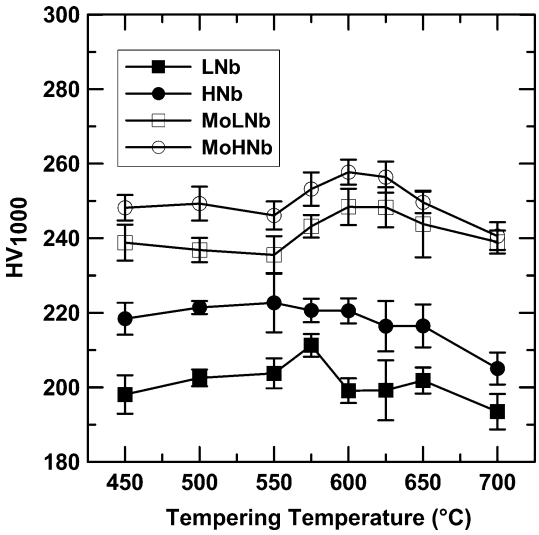

Fig. 7—Mean Vickers hardness for hot-rolled alloys following tempering for 120 min at temperatures between 723 K and 973 K (450 °C and 700 °C) (1 kg load, 10 s dwell time). Error bars indicate the standard deviation of 10 measurements.

In contrast to hot-rolled alloys, the coarsening rates for the previously solutionized LNb and MoLNb alloys at 1323 K, 1373 K, and 1423 K (1050 °C, 1100 °C, and 1150 °C) are approximately equal to or less than the values predicted by the LSW equation as shown in Figure 9(d). The previously tempered alloys also show a marked reduction in precipitate size after soaking at elevated temperature relative to hot-rolled alloys for times of 90 minutes at 1323 K (1050 °C) and 60 minutes at 1373 K (1100 °C) (Figures 9(a) through (c)). The reduction of the precipitate coarsening rate in the previously solutionized alloys and the reduced average precipitate radius in previously tempered alloys suggest that the enhanced and non-constant coarsening rates in hot-rolled alloys are due to the difference in starting precipitate size distributions, developed prior to reheating to elevated temperatures, between hot-rolled alloys, solutionized alloys, and tempered alloys. The variability in precipitate coarsening rates during holding in the austenite regime due to alloy composition and thermal processing differences warranted further investigation of the evolution of the PSDs during the entire thermal processing sequence.

The starting PSDs for hot-rolled and solutionized MoLNb are shown for comparison in Figure 10(a). Following the solutionizing treatment, only a small number density, n, of larger, cuboidal TiN precipitates remained in the solutionized MoLNb alloy, whereas the hot-rolled MoLNb alloy contains a higher number density of complex precipitates of spheroidal and mixed morphology in a bimodal distribution. Here, bimodality is defined by the relative peak heights, qualitatively, of fine and coarse precipitate distributions. For example, maximum bimodality is obtained when the peak heights of both distributions are equal. Note that PSDs are normalized by their respective precipitate count in Figure 10 and subsequent PSDs; therefore, neither precipitate number density nor volume fraction (related to observed areal density) can be compared from the plots. The number density of coarse precipitates (greater than 20 nm) in hot-rolled MoLNb, for example, is

Table III. Lineal Intercept Standard Deviation (σ) and Mean (μ) of Austenite Grains in Hot-Rolled Alloys Following Reheat to 1373 K (1100 °C) and Water Quench

	σ (μm)	μ (μm)	σ/μ
LNb	13.8	21.6	0.64
HNb	8.8	18.1	0.49
MoLNb	9.3	19.0	0.49
MoHNb	8.0	16.9	0.47

Table IV. Mean Lineal Intercept of Austenite Grains in Alloys Tempered and Solutionized Prior to Soaking

Alloy	Starting Condition	1323 K (1050 °C) for 90 min (μm)	1373 K (1100 °C) for 60 min (μm)
LNb	tempered	16.9	44.9
HNb	tempered	16.8	18.9
MoLNb	tempered	17.0	25.0
MoHNb	tempered	16.5	17.2
MoLNb	solutionized	—	25.8

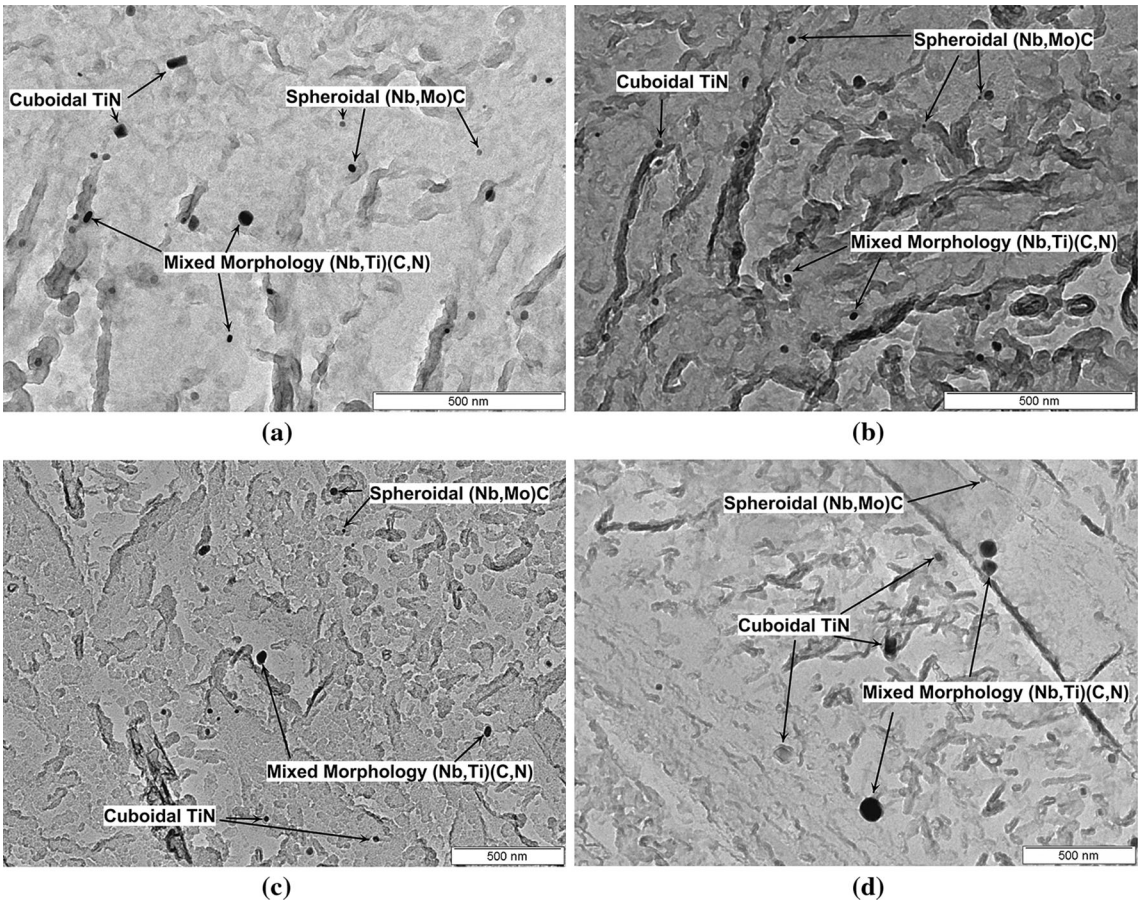

Fig. 8—Representative TEM micrographs of hot-rolled MoLNb reheated to 1373 K (1100 °C) and held for (*a*) 0 min, (*b*) 6 min, (*c*) 30 min, and (*d*) 60 min.

greater than that of solutionized MoLNb in Figure 10(a) despite a lower frequency of observation when normalized to total number of precipitates in the hot-rolled MoLNb condition. The initial bimodal PSD character of hot-rolled alloys is significantly different than the unimodal, self-consistent distribution assumed by the LSW model, and it develops as follows. A distribution of coarse precipitates (diameters greater than 20 nm) develops prior to and during soaking at 1523 K (1250 °C), hot-rolling, and cooling through the high-temperature austenite phase region. This distribution consists of complex (Nb,Ti)(C,N) precipitates of mixed spheroidal/cuboidal morphology and TiN precipitates of cuboidal morphology. As the hot-rolled alloy cools in the austenite and ferrite phase fields, a second distribution of fine precipitates (diameters less than 20 nm) consisting of NbC and (Nb,Mo)C of spheroidal morphology nucleates and grows to produce a bimodal starting PSD.[43]

It is hypothesized that the reduction in the volume number density of coarse precipitates and the reduced bimodality, *i.e.*, the absence of fine precipitates, of the initial PSD in the solutionized MoLNb condition result in a reduction in the coarsening rate and bimodality of the PSD after reheating to 1373 K (1100 °C) relative to the hot-rolled MoLNb as shown by comparison of Figures 10(b) and (c). In the hot-rolled alloys, the instability and dissolution of the fine precipitate population is enhanced by the presence of the coarse precipitates upon reheating to elevated temperature, and a rapid increase in average precipitate radius during soaking results. If coarse precipitates containing Nb are not present in appreciable number density, as in solutionized MoLNb, the coarsening rate is greatly reduced. High Nb samples (Figures 10(d) and (e)) exhibit a greater degree of bimodality and an associated increase in coarsening rate relative to low Nb samples, because coarse Nb-bearing precipitates are not fully solutionized at 1523 K (1250 °C) prior to hot-rolling; this difference in bimodality likely explains the unexpectedly large difference in coarsening rates between the HNb and LNb specimens.

To further characterize the effect of Mo on precipitate size distribution evolution during thermal processing, the effect of Mo on PSD evolution during reheating prior to holding in the austenite regime was investigated. The addition of Mo exhibits no noticeable effect on the PSD during heating prior to holding at 1373 K (1100 °C) as evidenced by comparison of Figures 10(d) and (e), which show the PSDs for the MoHNb and HNb alloys after heating to 1373 K (1100 °C) and quenching immediately.

Because tempering at 873 K (600 °C) for 120 minutes prior to reheating also enhances grain refinement and

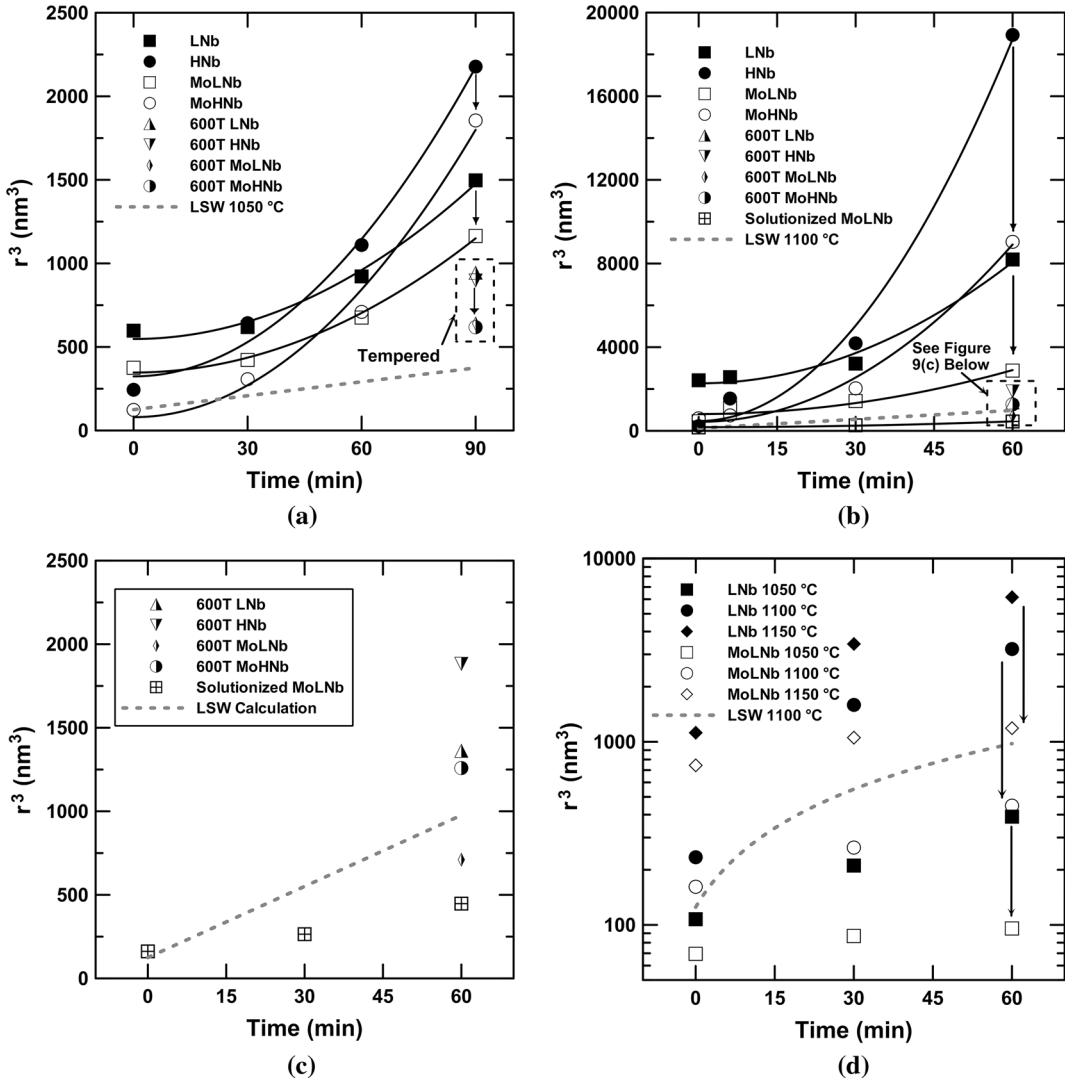

Fig. 9—Cube of the average precipitate radius (r^3) as a function of soaking time and thermal history at (*a*) 1323 K (1050 °C) and (*b*) 1373 K (1100 °C). Arrows indicate the reduction in mean precipitate radius due to Mo. Specimens tempered for 120 min at 873 K (600 °C) prior to reheating to elevated temperature are identified as 600T in all figures. Specimens tempered and soaked at 1373 K (1100 °C) are shown separately in (*c*) for clarity. LNb and MoLNb specimens solutionized and then soaked at 1323 K, 1373 K, and 1423 K (1050 °C, 1100 °C, and 1150 °C) are shown separately in (*d*). Solid lines in (a) and (b) are parabolic fits to hot-rolled and reheated alloy data, and LSW predictions for precipitate size are shown as dashed lines in each plot for comparison. Errors of ±13 nm^3 for each datum are estimated from a diameter measurement error of ±4 pixels. A minimum of 300 precipitates were measured for each condition. Note differences in vertical and horizontal axes.

reduces the rate of precipitate coarsening at elevated temperature, the effect of tempering on starting PSDs (prior to reheating) was investigated. The hot-rolled and tempered PSDs for MoLNb and MoHNb are shown in Figures 11(a) and (b), respectively. In both MoLNb and MoHNb, tempering results in an increase in both the average size and, presumably, the volume fraction of precipitates because full precipitation is unlikely to occur during cooling following hot-rolling as evidenced by the secondary hardening results of Section III–B. A corresponding decrease in solute Nb following tempering is expected. As hypothesized above, precipitate coarsening is likely enhanced by the co-presence of coarse and fine precipitates (or bimodality of the PSD) upon reheating to elevated temperature; thus, coarsening of the fine precipitates prior to reheat reduces capillary effects responsible for coarsening and delays the eventual dissolution of fine precipitates. Alternatively stated, coarsening of fine precipitates, increased volume fraction of precipitates, and an associated reduction in solute Nb, result from the tempering of hot-rolled alloys. The coarsening rates of tempered specimens at elevated temperatures are accordingly reduced relative to hot-rolled specimens.

Further analysis was conducted to quantify the bimodal character of the hot-rolled precipitate size distributions. A representative precipitate size distribution evolution is shown in Figure 12 for hot-rolled MoHNb held at 1373 K (1100 °C) for various times. Precipitate diameter distributions have been fit to the probability distribution function, y, of two offset log-normal distributions shown in Eq. [4].

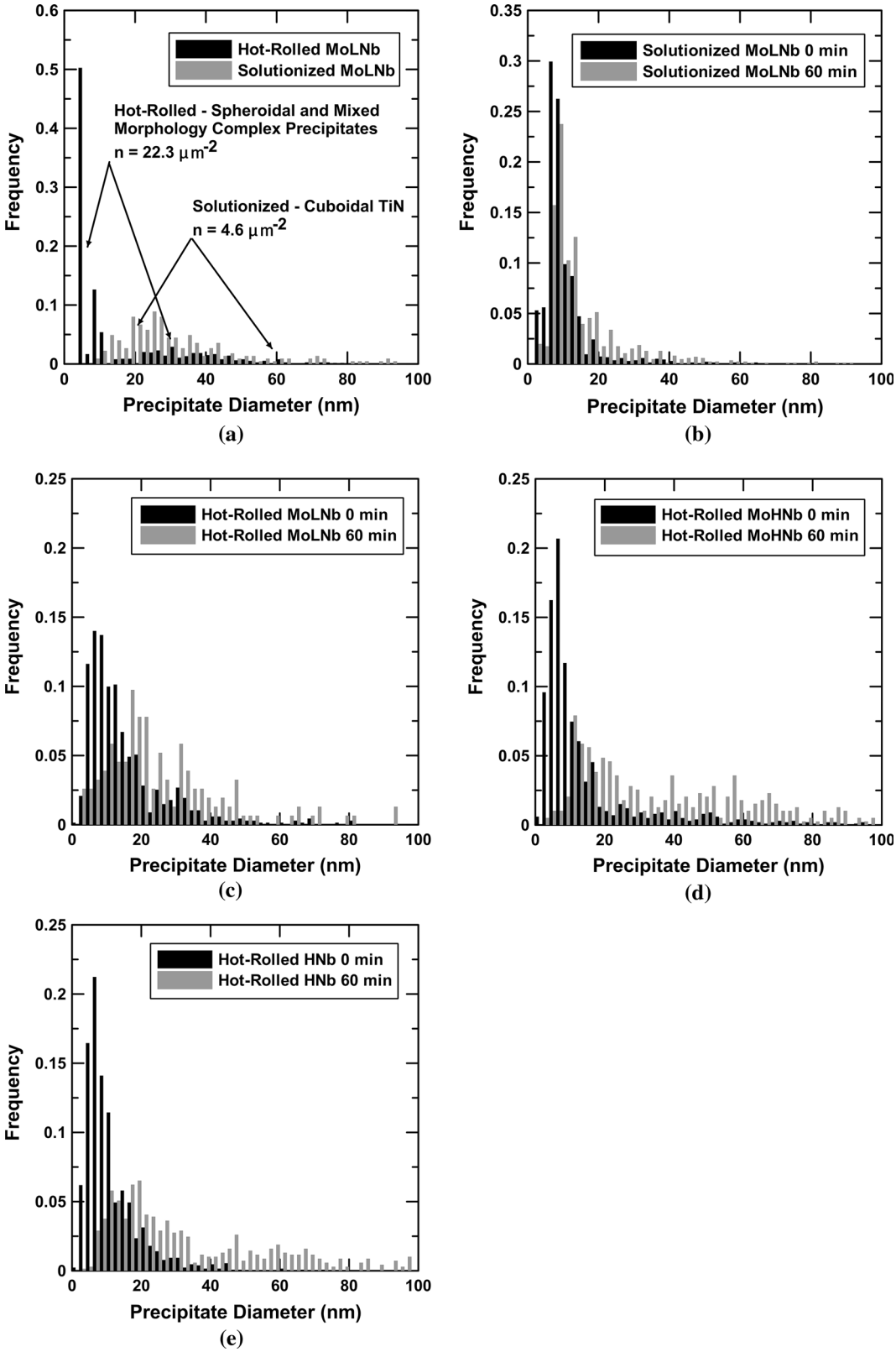

Fig. 10—Precipitate size distributions for (*a*) hot-rolled and solutionized MoLNb prior to reheating, and precipitate size evolutions of (*b*) solutionized MoLNb, (*c*) hot-rolled MoLNb, (*d*) hot-rolled MoHNb, and (*e*) hot-rolled HNb for specified times at 1373 K (1100 °C). Bin sizes are 2 nm. A minimum of 300 precipitates were measured for each condition. Note differences in vertical axes.

Table V. Parameters Used for LSW Calculation in Austenite

	$\gamma_{P/M}$ (J/m^2)[3]	Ω (m^3/mol)[3]	[Nb] at 1323 K (1050 °C) (At Frac)[57]	[Nb] at 1373 K (1100 °C) (At Frac)[57]	[Nb] at 1423 K (1150 °C) (At Frac)[57]	D_{Nb} at 1323 K (1050 °C) (m^2/s)[3]	D_{Nb} at 1373 K (1100 °C) (m^2/s)[3]	D_{Nb} at 1423 K (1150 °C) (m^2/s)[3]
LNb	0.8	6.7×10^{-6}	7.8×10^{-5}	1.3×10^{-4}	2.1×10^{-4}	1.31×10^{-15}	4.11×10^{-15}	1.21×10^{-14}
HNb	0.8	6.7×10^{-6}	8.3×10^{-5}	1.4×10^{-4}	—	1.31×10^{-15}	4.11×10^{-15}	—
MoLNb	0.8	6.7×10^{-6}	7.8×10^{-5}	1.3×10^{-4}	2.2×10^{-4}	1.31×10^{-15}	4.11×10^{-15}	1.21×10^{-14}
MoHNb	0.8	6.7×10^{-6}	8.3×10^{-5}	1.4×10^{-4}	—	1.31×10^{-15}	4.11×10^{-15}	—

Table VI. Ratios of Observed Coarsening Rates to Calculated Lifshitz-Slyozov-Wagner Coarsening Rates

Alloy	Starting Condition	1323 K (1050 °C)	1373 K (1100 °C)	1423 K (1150 °C)
LNb	hot-rolled	3.8	6.9	—
HNb	hot-rolled	7.4	22	—
MoLNb	hot-rolled	3.3	2.7	—
MoHNb	hot-rolled	6.5	10	—
LNb	solutionized	1.8	1.8	1.3
MoLNb	solutionized	0.16	0.17	0.12

$$y = \sum_{i=1}^{2} f((x - a_i)|\mu_i, \sigma_i, f_i) = \sum_{i=1}^{2} \frac{f_i}{(x - a_i)\sigma_i\sqrt{2\pi}} e^{\frac{-(\ln(x-a_i)-\mu_i)^2}{2\sigma_i^2}}; \qquad f_2 = 1 - f_i, \quad [4]$$

where a_i, μ_i, f_i, and σ_i are the offset, location parameter, weighting parameter, and scale parameter of the ith log-normal distribution. The mean diameter of the first distribution, the mean diameter of the second distribution, and the arithmetic weighting of the second (coarser) distribution are given by d_1, d_2, and f_2, respectively, in Figures 12(a) and (b). Figure 12(c) illustrates the evolution of fits to MoHNb PSDs following soaking at 1373 K (1100 °C) for times of 0, 6, 30, and 60 minutes. All fit values for d_1, d_2, and f_2 for hot-rolled alloys increase monotonically with time at an soaking temperature of 1373 K (1100 °C) as shown in Table VII, and the distribution becomes more bimodal with time due to precipitate shrinkage below the average precipitate diameter and precipitate growth above the average diameter. Here, bimodality is a sufficient pre-condition for enhanced coarsening during soaking in austenite, but it is not a necessary pre-condition. Alternatively stated, any PSD that is not self-consistent and unimodal, similar to the solution to the LSW equation, will be unstable, coarsen at an enhanced rate, and tend toward a unimodal, self-consistent distribution in which the mode is necessarily greater than the mean. The mean diameters of the PSD fits shown in Figures 12(a) and (b) correspond to inflection points generated by dissolution below and growth above the mean diameter.

To complement the hypotheses above, MatCalc© was employed to qualitatively assess the effect of prior precipitate distributions on the evolution of Nb-rich carbides during reheating and soaking in austenite of a model HNb alloy (Fe-0.20 C-0.10 Nb-0.015 Ti-0.009 N wt pct). A bimodal precipitate distribution, as shown in Figure 13(a), was developed by simulating soaking at 1573 K (1250 °C) for 120 minutes followed by a slow quench to room temperature (2 K/s) to use as a comparison to a fully solutionized condition prior to reheating. The coarse precipitate mode of the bimodal distribution was developed during soaking at 1523 K (1250 °C), and the finer precipitate mode was developed during quenching to room temperature as indicated. Precipitates that were nucleated in austenite and ferrite are shown separately in Figure 13(a). The average precipitate radius is shown for both simulated conditions as a function of time during the simulated reheating and soaking cycle in Figure 13(b). Temperature during the reheating and soaking cycle is shown as a function of time for reference. The prior bimodal precipitate distribution results in an enhanced observed coarsening rate relative to the fully solutionized condition (no PSD prior to reheating) during ramping to 1373 K (1100 °C) and subsequent soaking as shown in Figure 13(b). Experimental precipitate size data from the HNb condition are plotted for comparison to simulation results in Figure 13(b), and the simulation results agree with experimental observation of increased coarsening rates relative to the LSW model (approximated by the fully solutionized specimen) for alloys with an initial bimodal precipitate size distribution. The slight reductions in the calculated average precipitate radius with time are an artifact of the simulation attributed to the discrete nature of the precipitate size distribution (rapid reduction in size of the smallest precipitate size class).

D. *Precipitate Composition Analyses*

Molybdenum additions have a distinct effect on the precipitate size distribution (PSD) evolution and associated austenite grain refinement. Both this and previous work have suggested that precipitate composition, Mo

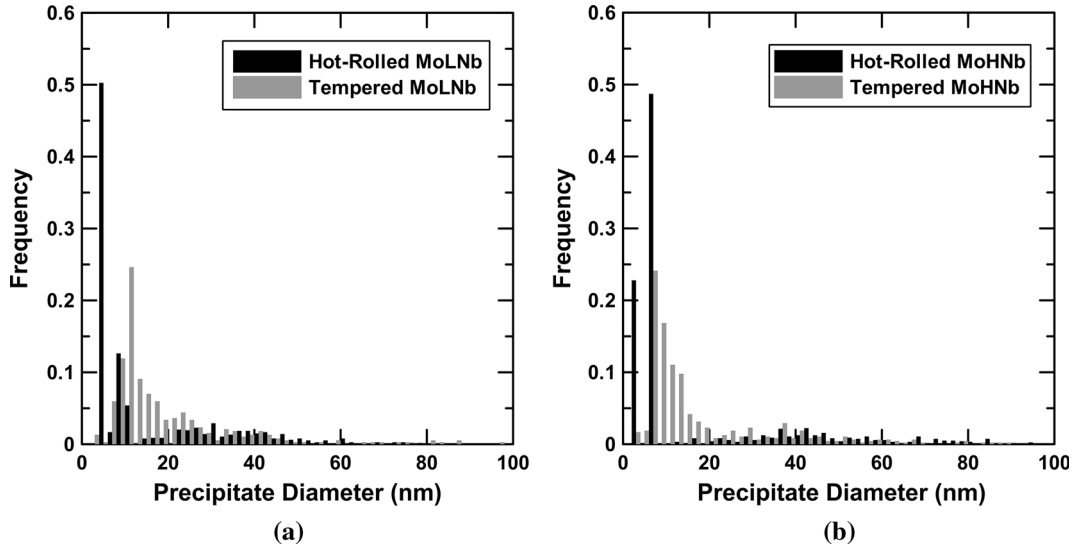

Fig. 11—Precipitate size distributions for (*a*) hot-rolled and tempered MoLNb and (*b*) hot-rolled and tempered MoHNb. Bin sizes are 2 nm. A minimum of 300 precipitates were measured for each condition.

as MoC incorporation specifically, may affect the PSD development at elevated temperature. Accordingly, precipitate compositions following hot-rolling and cooling and during soaking were investigated with special focus placed on Mo incorporation. The results of these investigations are summarized below and in previously reported work.[43]

To determine the possible effect of Mo on solute Nb in hot-rolled alloys prior to reheating, as this is thought to influence the PSD developed during reheating to elevated temperature, electrochemical dissolution, and precipitate extraction investigations were conducted on hot-rolled specimens. The hot-rolled Mo-containing alloys contain weight fractions of Mo on the carbide metallic sublattice of 0.37 ± 0.011 and 0.14 ± 0.006 for the MoLNb and MoHNb alloys, respectively. Figure 14 shows the experimentally determined fraction of Nb in solution in hot-rolled alloys. The HNb alloy has a greater fraction of solute Nb than the LNb alloy in the hot-rolled condition. Because the equilibrium amount of solute Nb at room temperature is expected to be small similar for the two Nb additions, this result indicates that the Nb-rich precipitate volume fraction is far from equilibrium following hot-rolling and cooling to room temperature. Molybdenum additions, despite their marked effects on austenite decomposition during cooling and possible effects on Nb-rich precipitate nucleation in ferrite,[54] have little effect on the fraction of Nb in solution prior to reheating for both levels of Nb evaluated.

Electrochemical dissolution and precipitate extraction was also performed on Mo-bearing alloys soaked in the austenite regime to observe Mo incorporation. Figure 15 shows the concentration of Mo on the metallic sublattice of extracted precipitates as measured by ICP-MS in specimens of MoLNb and MoHNb reheated to 1373 K (1100 °C) and held for times of 0, 30, and 60 minutes. As shown, Mo concentrations are reduced in both MoLNb and MoHNb specimens with holding time at 1373 K (1100 °C), presumably due to dissolution of the finer, Mo-rich precipitate distribution and Mo rejection to the austenite matrix, and Mo incorporation is greater in the low Nb alloy. The dissolution and precipitate extraction investigations support previously reported modeling and experimental evidence of Mo instability in carbonitrides at elevated temperature in austenite.[43]

Solute Nb and precipitated Nb during soaking at 1373 K (1100 °C) were also investigated by electrochemical dissolution and precipitate extraction. Figures 16(a) and (b) show solute Nb, and Figures 16(c) and (d) show precipitated Nb as a function of holding time at 1373 K (1100 °C). Only slight increases, within the calculated errors, are observed in solute Nb concentration as a function of time during holding at 1373 K (1100 °C) as shown in Figures 16(a) and (b). The Nb fractions in extracted precipitates decrease only slightly during soaking as shown in Figures 16(c) and (d), and these results indicate that rapid growth and dissolution processes do not play a significant role in the PSD evolution at 1373 K (1100 °C). Alternatively stated, coarsening is the primary means of PSD evolution during soaking at 1373 K (1100 °C). Lastly, no systematic difference in the solute Nb concentration is observed with additions of Mo in the experimental alloys. The difference between precipitated Nb amounts in HNb and MoHNb shown in Figure 16(d) is attributed to the difference in total Nb additions (0.104 wt pct Nb in HNb and 0.118 wt pct Nb in MoHNb).

The various mechanisms that may contribute to the reduction of the Nb-rich precipitate coarsening rate and associated reduction in austenite grain growth during elevated temperature processing due to Mo additions are discussed further in the following section.

E. *Mechanisms of Reduction of Nb-Rich Precipitate Coarsening Due to Mo*

Although no one individual mechanism was identified for the observed reduction in microalloy precipitate

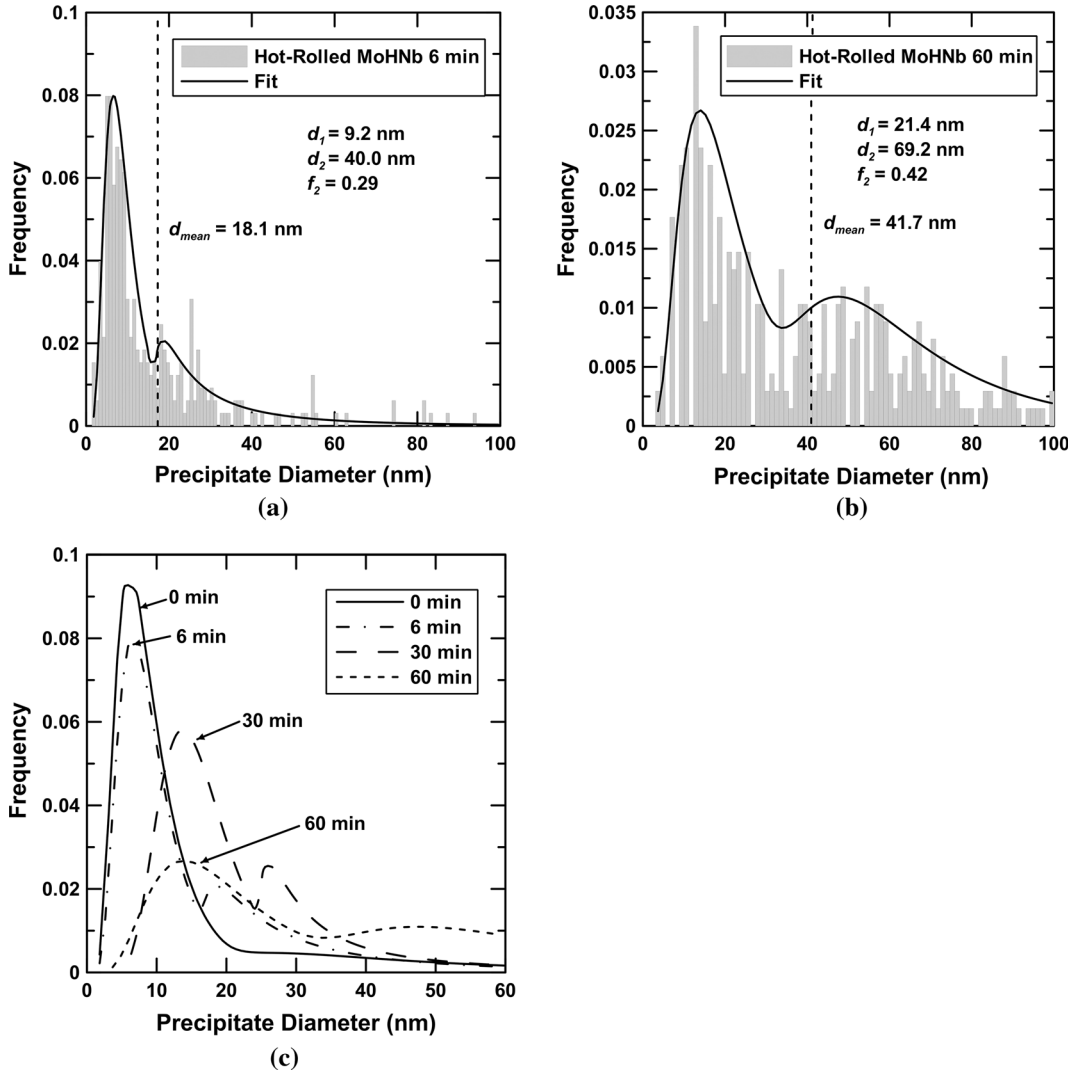

Fig. 12—Precipitate diameter distributions for the MoHNb hot-rolled alloy following holding times of (*a*) 6 min and (*b*) 60 min at 1373 K (1100 °C). Precipitate size distributions were fit to the superposition of two offset log-normal distributions as indicated by the trend-lines in the above figure (*c*) for MoHNb soaked at 1373 K (1100 °C) for various times. The mean diameter of the first distribution, mean diameter of the second distribution, and arithmetic weighting of the second distribution are given by d_1, d_2, and f_2, respectively, in (a) and (b). All values increase monotonically with soaking time, and the distribution becomes more bimodal with time. Bin sizes are 1 nm. A minimum of 300 precipitates were measured for each condition. Note differences in vertical axes.

Table VII. Fit Parameters for Precipitate Size Distributions of Alloys Developed During Soaking at 1373 K (1100 °C)

	d_1 (0 min) (nm)	d_1 (60 min) (nm)	d_2 (0 min) (nm)	d_2 (60 min) (nm)	f_2 (0 min)	f_2 (60 min)
LNb	20.6	27.1	58.8	59.8	0.16	0.44
HNb	9.4	23.1	31.2	104.6	0.13	0.34
MoLNb	12.3	22.6	37.3	38.7	0.12	0.36
MoHNb	9.2	21.4	40.0	69.2	0.29	0.42

coarsening rates due to the addition of Mo, it was established that this reduction results in reduced austenite grain growth at the tested temperatures. Possible alternative mechanisms are summarized to the extent of current understanding and in light of presented data in the following sections. Additional analyses are required beyond those employed in this work to determine the relative contributions of the described mechanisms.

1. *Mo Segregation to the Precipitate-Matrix Interface*

Previous studies have suggested that Mo may segregate to the precipitate-matrix interface and reduce precipitate coarsening rates, either by reducing the precipitate-matrix surface energy or by reducing the precipitate-matrix interface mobility through solute drag.[40,42] It is clear from precipitate coarsening rates presented in Sections III–A and III–B that Mo reduces

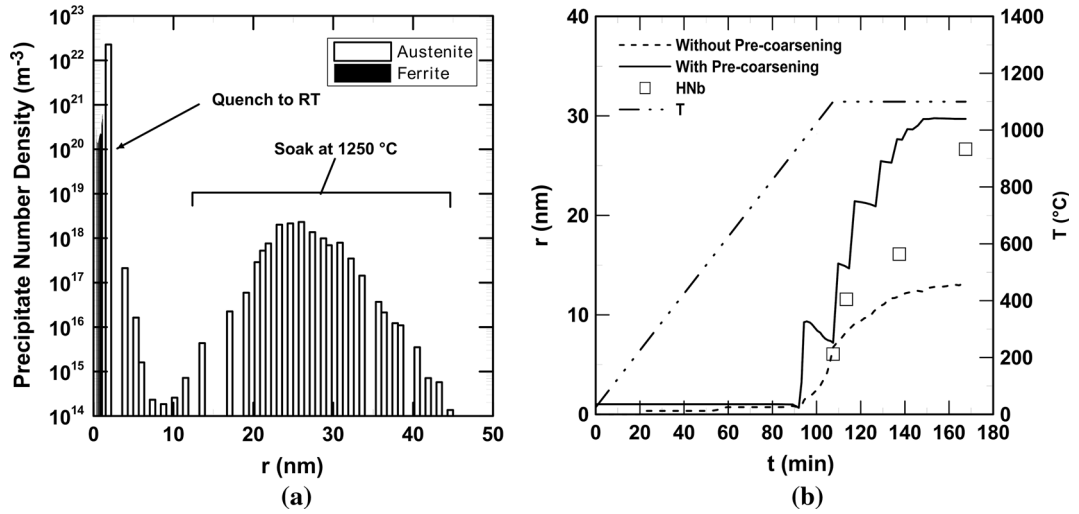

Fig. 13—(*a*) Predicted pre-coarsened precipitate radius distribution of a model HNb alloy soaked at 1523 K (1250 °C) for 120 min followed by cooling to room temperature at 2 K/s. The phase in which the precipitates nucleated is identified in the distribution. (*b*) Calculated average radius, *r*, as a function of time, *t*, for a model HNb alloy during ramp at 10 K/min and soak at 1373 K (1100 °C). The radius evolution is calculated for both the pre-coarsened and non-pre-coarsened conditions and is compared to the experimentally determined radius evolution in the HNb alloy. The temperature axis is shown on right for the reheating schedule.

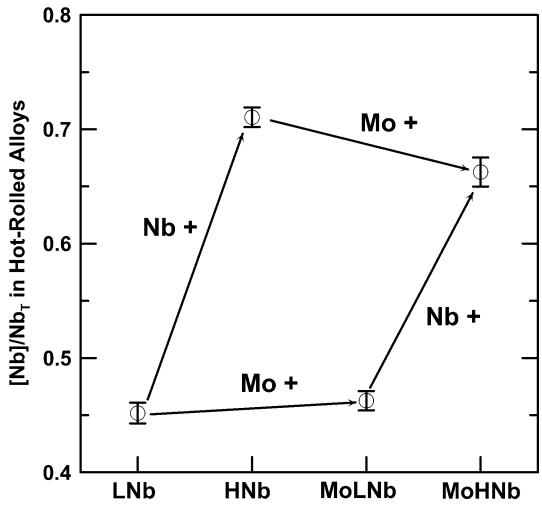

Fig. 14—Ratio of solute Nb to total Nb by weight in the experimental hot-rolled alloys. The effects of increased Nb and Mo additions are indicated by arrows. The error bars denote standard deviation of four measurements.

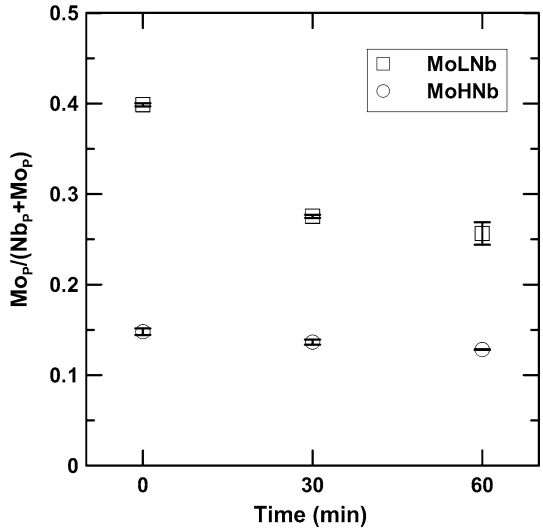

Fig. 15—Fractional concentration of Mo by weight on the metallic sublattice of precipitates extracted from MoLNb and MoHNb specimens reheated to 1373 K (1100 °C) and held for times of 0, 30, and 60 min. Note the reduction of Mo concentration with time. Error bars denote the standard deviation of four measurements.

the austenite grain growth and precipitate coarsening rates in experimental alloys, but no clear evidence of Mo segregation to the precipitate-matrix interface was obtained from previous scanning TEM or atom probe tomography investigations.[43] If a monolayer of Mo were to exist at the precipitate-matrix interface, however, it is unclear if current analytical techniques are sensitive enough to distinguish this monolayer from Mo incorporated in the precipitate during precipitate growth and coarsening. For this reason, the presence of Mo segregation to the precipitate-matrix interface cannot be dismissed as a possible mechanism, but the presence of such segregation has yet to be verified.

2. *Mo Incorporation and Effects on Interfacial Energy and Nucleation*

Recently published calculations by Jang *et al.* suggest that replacement of Ti by Mo on the metallic sublattice of B1 carbides in ferrite results in a reduction in precipitate-matrix interfacial stress in coherent precipitates and may aid in the early stages of nucleation of (Ti,Mo)C in ferrite. A similar hypothesis may be put forward for the incorporation of Mo in Nb-rich carbonitrides in ferrite and/or austenite.

If coherency stress reduction of (Nb,Mo)C in ferrite is responsible for the observed reduction in precipitate coarsening rate due to Mo additions, the effect would be

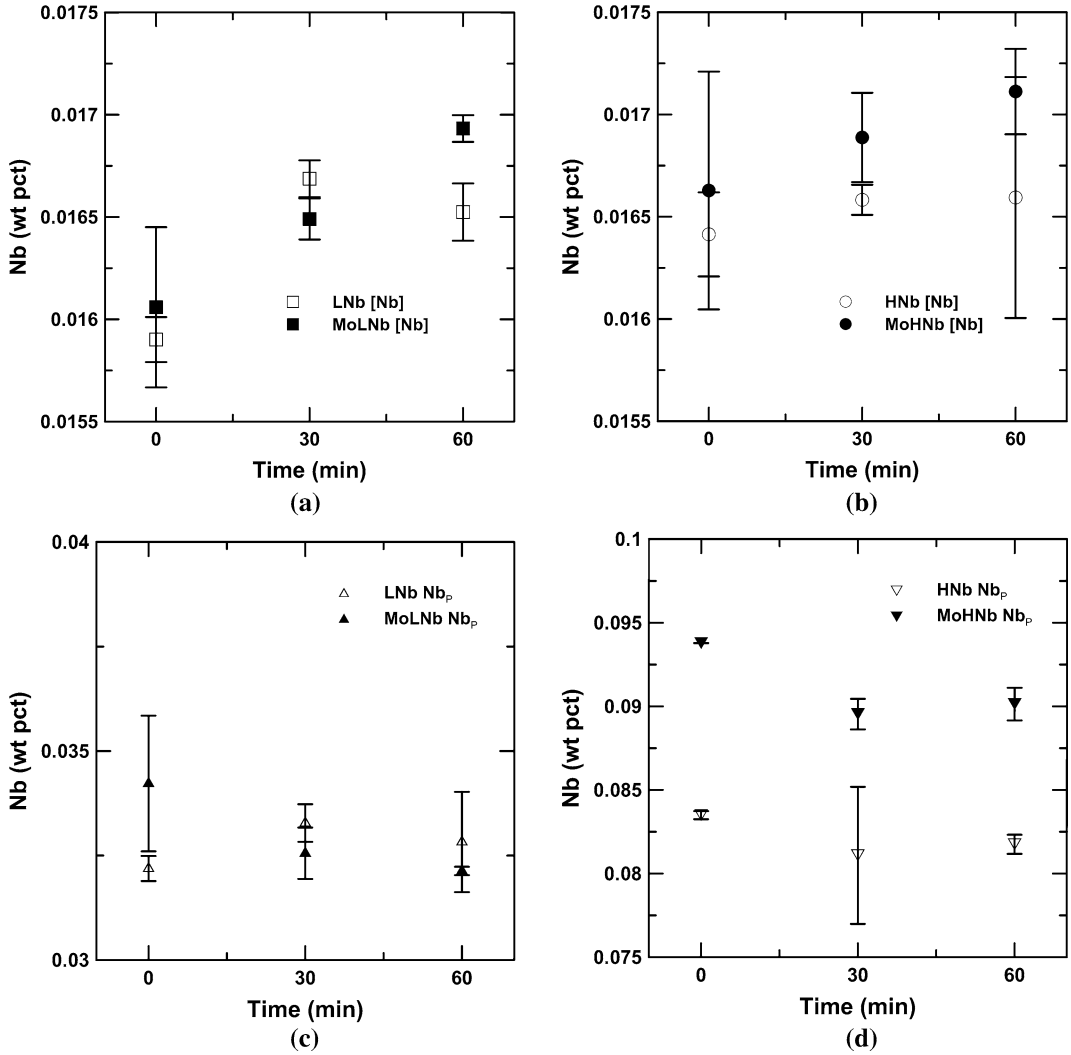

Fig. 16—Solute Nb, *[Nb]*, in (*a*) low Nb and (*b*) high Nb alloys, and Nb incorporated in extracted precipitates, Nb_P, in (*c*) low Nb and (*d*) high Nb alloys as a function of holding time at 1373 K (1100 °C). Error bars denote the standard deviation of four measurements. Note differences in vertical axes.

most prominent during reheating in ferrite to soaking temperatures. Reduced coherency stress would reduce the dissolution rate of the fine mode of the precipitate size distribution (PSD) during reheating in ferrite, although coherency would be lost during transformation to austenite. Coarse precipitates in austenite prior to reheating are assumed incoherent. From Figures 10(d) and (e), however, it is clear that MoHNb and HNb specimens display similar PSDs following reheating to 1373 K (1100 °C). For this reason, the effects of Mo on interfacial stresses during nucleation and the early stages of growth in ferrite are not thought to be of great importance in PSD evolution during reheating.

Alternatively, incorporation of Mo into Nb-rich precipitates as MoC could produce a reduction in precipitate coarsening rates in austenite through the mechanism of precipitate reversion, in which coherent precipitates nucleated in ferrite are quickly dissolved following transformation to austenite during reheating due to the loss of interface coherency.[63,64] Previous calculations[43] suggest that Mo incorporation during precipitation in ferrite increases the solubility of precipitates relative to Mo-free precipitates in austenite, and accelerated dissolution would be followed by coherent re-precipitation of more Nb-rich precipitates in austenite. The reduction in precipitate coarsening rate in Mo-bearing alloys, in this instance could be attributed to reduced interfacial energies of fine precipitates associated with precipitate-austenite matrix coherency. The interfacial energies for coherent and incoherent particles in ferrous systems are generally in the range of 0.1-0.2 J/m^2 and 0.5-1.2 J/m^2,[4] respectively, and the difference between these energies would be of the order necessary to achieve coarsening rate reductions of ~90 pct between LNb and MoLNb (Table VI).

It may also be suggested that the incorporation of Mo may reduce the interfacial energy of incoherent Nb-rich precipitates during coarsening in ferrite and austenite and reduce precipitate coarsening rates. Any additional conclusions, though, related to the possible effect of Mo incorporation on precipitate-matrix surface energy in austenite are speculative. It does not appear likely, given

the generally reported range of interfacial energies of incoherent particles in iron, that Mo incorporation on the metallic sublattice of Nb-rich precipitates could be solely responsible for such a pronounced decrease in precipitate-matrix surface energy and associated precipitate coarsening rate.

Secondary hardening investigations presented in Section III–B lend support to the beneficial effect of Mo incorporation in nucleation and growth of Nb-rich precipitates in ferrite. As shown, Mo-containing alloys display distinct secondary hardening peaks after tempering for 120 minutes at 873 K to 898 K (600 °C to 625 °C), whereas Mo-free alloys display no distinct secondary hardening. This behavior cannot be due to differences in solute Nb prior to tempering because Mo does not have a significant effect on solute Nb in hot-rolled alloys as shown in Figure 14. Despite clear effects of Mo on secondary hardening behavior in ferrite, it is not immediately obvious how these findings relate to similar effects on precipitate nucleation, growth, and coarsening in austenite.

3. *Reduction in Nb Diffusivity Due to Mo Addition*

Previous studies have suggested that Mo may reduce the diffusivity of Nb in austenite and, thereby, reduce the rate of precipitate coarsening by long-range diffusion.[13–15] It is entirely feasible that Mo may reduce the frequency factor of Nb diffusion in austenite by reducing the number of vacancy exchanges with Nb atoms through a mechanism of preferential exchange. Any conclusions to this effect are speculative, but similar suggestions have been made for the effect of Mn on Nb diffusion in austenite by Kurokawa *et al.*, although an addition of 1.5 wt pct Mn in 99.99 wt pct pure Fe was only shown to reduce the frequency factor by ~15 pct with no change in the diffusion activation energy.[15] In order to explain the entire coarsening rate difference (Nb diffusion rate) between the Mo-bearing and Mo-free alloys, the frequency factor would have to be reduced by ~90 pct due to the addition of Mo. However, such a reduction has not been reported in literature for any substitutional element in austenite.

4. *Mo Partitioning to Austenite During Holding at Elevated Temperatures*

Electrochemical dissolution and precipitate extraction investigations have shown that Mo incorporation into precipitates decreases with isothermal soaking time in austenite. Precipitate coarsening rates may be reduced, if Mo partitioned from the precipitate during holding in austenite reduces either the incorporation of Nb into the coarse precipitates from austenite or rejection of Nb from the fine precipitates to austenite. This could possibly occur by an effect of Mo on Nb activity or diffusivity in the austenite region immediately surrounding the precipitate. The possible diffusivity or activity effects of Mo on Nb may be enhanced with elevated Mo concentrations around a coarsening precipitate due to partitioning.

IV. CONCLUSIONS

A. *Effects of Mo and Nb on Austenite Grain Size Evolution*

The prior austenite grain size of Mo-bearing alloys is reduced relative to the Mo-free alloys at extended soaking times at 1323 K and 1373 K (1050 °C and 1100 °C). Mo-bearing alloys also display greater grain size uniformity relative to Mo-free alloys upon reheating to 1373 K (1100 °C). High Nb alloys (HNb and MoHNb) are much more capable of retarding the onset of abnormal growth when compared to the low Nb alloys (LNb and MoLNb). Additions of Mo and Nb, therefore, are both beneficial in delaying the onset and extent of abnormal grain growth in reheated and soaked hot-rolled alloys.

B. *Effects of Mo and Nb on Precipitate Size and Composition Evolution*

Molybdenum additions result in a significant decrease in precipitate coarsening rate in all tested conditions relative to Mo-free alloys. An increase in Nb concentration increases the precipitate coarsening rate. Little effect on the solute Nb fraction is observed in hot-rolled alloys due to Mo additions. Molybdenum concentration in precipitates is reduced in both MoLNb and MoHNb alloys with holding time at 1373 K (1100 °C), presumably due to partial dissolution of the finer, Mo-rich precipitate distribution and partitioning of Mo to the austenite matrix. The observed reduction of the Mo concentration in precipitates with time during isothermal soaking is in agreement with previous published scanning TEM investigations.[43]

C. *Effects of Thermal History on Precipitate Size and Austenite Grain Size Evolution*

During holding at elevated temperature, a rapid increase in average the Nb-rich precipitate radius in previously hot-rolled alloys is observed relative to LSW predictions. It is hypothesized that the instability and associated dissolution of the fine precipitate population formed during slow cooling and/or reheating is enhanced by the presence of the coarse precipitates in the initial precipitate size distribution (PSD). Quantitative modeling results, shown in Figure 13, support this hypothesis. This accelerated coarsening mechanism has not been previously identified in literature concerning particles in ferrous systems.

Tempering at 873 K (600 °C) for 120 minutes greatly reduces the austenite grain size of all experimental alloys following soaking at 1323 K and 1373 K (1050 °C and 1100 °C) relative to hot-rolled alloys, and abnormal grain growth is effectively eliminated in all specimens held for 90 minutes at 1323 K (1050 °C). Specimens tempered prior to reheating to elevated temperature show decreased average precipitate radii for the times at which they are tested, and Mo is shown to further decrease the average precipitate radius for a given Nb concentration at each holding time. It is hypothesized

that coarsening is enhanced in hot-rolled alloys by the co-presence of coarse and fine precipitates upon reheating to elevated temperature; thus, any stabilization (growth and coarsening) of the fine precipitates prior to reheat decreases the bimodality of the PSD, reduces capillary effects responsible for coarsening, and delays the eventual dissolution of fine precipitates due to the coarse precipitates.

Like tempering prior to reheating, solutionizing of MoLNb prior to reheating reduces the measured grain size relative to the hot-rolled condition. In addition, abnormal grain growth is not present in solutionized and reheated MoLNb after soaking at 1373 K (1100 °C) for 60 minutes. Reduction in the number density of coarse, Nb-rich precipitates of the initial PSD in the solutionized MoLNb also results in a reduction in the coarsening rate and bimodality of the PSD after reheating relative to the hot-rolled MoLNb.

D. *Mechanism of Mo Effects on Precipitate Coarsening in Austenite*

The results indicate that Mo addition does not significantly affect the solute Nb concentration in hot-rolled alloys or upon reheating and holding in austenite. Previous investigations report no distinct Mo enrichment of the precipitate-austenite matrix interface and do not provide clear support of the hypothesis that Mo reduces the coarsening rate of microalloy carbonitrides in austenite through this mechanism as reported previously for ferrite.[43] The incorporation of Mo as MoC into precipitates may reduce the precipitate-matrix surface energy, but the surface energy reduction necessary to achieve the observed reductions in coarsening rates appears implausible for incoherent precipitates. Incorporation of Mo into Nb-rich precipitates could reduce precipitate coarsening rates in austenite, however, if Mo enhances the mechanism of precipitate reversion, resulting in a greater fraction of coherent precipitates in austenite. Molybdenum additions may also reduce the precipitate coarsening rates by reducing the frequency factor for Nb diffusion.

ACKNOWLEDGMENTS

The authors are grateful for the financial support of the Advanced Steel Processing and Products Research Center at the Colorado School of Mines and its industrial sponsors. This work was partially supported by the EAPSI Program of the National Science Foundation as and the JSPS Summer Program under Award No. OISE-1107789. This work was also partially supported by the IMI Program of the National Science Foundation under Award No. DMR 0843934. Special thanks are extended to Professor Bruno De Cooman of the Graduate Institute of Ferrous Technology at POSTECH, and Professor Nobuhiro Tsuji of Kyoto University.

REFERENCES

1. J.P. Wise, D.K. Matlock, and G. Krauss: in *Heat Treating: Proceedings of the 20th Conference*, K. Funatani and G. E. Totten, eds., ASM International, Metals Park, OH, 2001, pp. 1152–61.
2. L.J. Cuddy and J.C. Raley: *Metall. Trans. A*, 1983, vol. 14A, pp. 1989–95.
3. T. Gladman: *Grain Size Control*, Maney Publishing, London, 2004.
4. T. Gladman: *The Physical Metallurgy of Microalloyed Steels*, Institute of Materials, London, 1997.
5. A.J. DeArdo: *International Materials Review*, 2003, vol. 48, pp. 371–402.
6. K.A. AlOgab, D.A. Matlock, and J.G. Speer: in *New Developments on Metallurgy and Applications of High Strength Steels*, T. Perez, ed., Tenaris, Ternium, and Argentina, Association of Materials, Buenos Aires, Argentina, 2008, p. 14.
7. K.A. AlOgab, D.K. Matlock, J.G. Speer, and H.J. Kleebe: *ISIJ Int.*, 2007, vol. 47, pp. 307–16.
8. T. Murakami, H. Hatano, Y. Shindo, M. Nagahama, and H. Yaguchi: *Mater. Sci. Forum*, 2007, vols. 539–543, pp. 4167–72.
9. T. Murakami, H. Hitoshi, and H. Yaguchi: in *Proceedings of the International Conference on New Developments in Long and Forged Products: Metallurgy and Applications*, J.G. Speer, E.B. Damm, and C.V. Darragh, eds., AIST, Warrendale, PA, 2006, pp. 99–106.
10. L. Ratke and P.W. Voorhees: *Growth and Coarsening: Ostwald Ripening in Material Processing*, 1st ed., Springer, New York, 2002.
11. D. San Martín, F.G. Caballero, C. Capdevila, and C. García de Andrés: *Mater. Sci. Forum*, 2005, vols. 500–501, pp. 703–10.
12. H. Zou and J.S. Kirkaldy: *Metall. Trans. A*, 1991, vol. 22A, pp. 1511–24.
13. M.G. Akben, B. Bacroix, and J.J. Jonas: *Acta Metall.*, 1983, vol. 31, pp. 161–74.
14. W.B. Lee, S.G. Hong, C.G. Park, and S.H. Park: *Metall. Mater. Trans. A*, 2002, vol. 33A, pp. 1689–98.
15. S. Kurokawa, E. Ruzzante, A.M. Hey, and F. Dyment: *Met. Sci.*, 1983, vol. 17, pp. 433–38.
16. Nerea. Isasti, Denis. Jorge-Badiola, Mitra.L. Taheri, and Pello. Uranga: *Metall. Mater. Trans. A*, 2014, vol. 45A, pp. 4960–71.
17. F.G. Wilson and T. Gladman: *Int. Mater. Rev.*, 1988, vol. 33, pp. 221–86.
18. S.S. Hansen, J.B. Vander Sande, and M. Cohen: *Metall. Trans. A*, 1980, vol. 11A, pp. 387–402.
19. J.G. Speer and S.S. Hansen: *Metall. Trans. A*, 1989, vol. 20A, pp. 25–38.
20. E.J. Palmiere, C.I. Garcia, and A.J. DeArdo: *Metall. Trans. A*, 1994, vol. 25A, pp. 277–86.
21. D San Martin, FG Caballero, C Capdevila, and CG de Andres: *Mater. Trans.*, 2004, vol. 45, pp. 2797–804.
22. K.A. AlOgab, D.K. Matlock, J.G. Speer, and H.J. Kleebe: *ISIJ Int.*, 2007, vol. 47, pp. 1034–41.
23. R.E. Thompson, D.K. Matlock, and J.G. Speer: *J. Mater. Manuf.*, 2007, vol. 116, pp. 392–407.
24. T. Murakami, H. Hitoshi, and H. Yaguchi: *Tetsu-to-Hagane*, 2006, vol. 92, pp. 38–46.
25. M.J. Cancio, G. Echaniz, and T.E. Perez: *Steel Res.*, 2002, vol. 73, pp. 340–46.
26. M. Charleux, W.J. Poole, M. Militzer, and A. Deschamps: *Metall. Mater. Trans. A*, 2001, vol. 32A, pp. 1635–47.
27. A.J. Craven, K. He, L.A.J. Garvie, and T.N. Baker: *Acta Mater.*, 2000, vol. 48, pp. 3857–68.
28. H. Zou and J.S. Kirkaldy: *Metall. Trans. A*, 1992, vol. 23A, pp. 651–57.
29. R.D.K. Misra, K.K. Tenneti, G.C. Weatherly, and G. Tither: *Metall. Mater. Trans. A*, 2003, vol. 34A, pp. 2341–51.
30. W. Wang and H.R. Wang: *Mater. Lett.*, 2007, vol. 61, pp. 2227–30.
31. S.G. Hong, K.B. Kang, and C.G. Park: *Scripta Mater.*, 2002, vol. 46, pp. 163–68.
32. Erik J Pavlina: Colorado School of Mines, 2011.
33. S. Okaguchi and T. Hashimoto: *Trans. ISIJ*, 1987, vol. 27, pp. 467–73.
34. R.M. Poths, R.L. Higginson, and E.J. Palmiere: *Scripta Mater.*, 2001, vol. 44, pp. 147–51.

35. K. Junhua, Z. Lin, G. Bin, L. Pinghe, W. Aihua, and X. Changsheng: *Mater. Des.*, 2004, vol. 25, pp. 723–28.
36. Z. Tang and W. Stumpf: *Mater. Charact.*, 2008, vol. 59, pp. 717–28.
37. G. Krauss: *Steels: Processing, Structure, And Performance*, 3rd ed., ASM International, Metals Park, 2005.
38. M.G. Akben, I. Weiss, and J.J. Jonas: *Acta Metall.*, 1981, vol. 29, pp. 111–21.
39. J.D. L'Ecuyer, D. L'Esperance, M.G. Akben, and B. Bacroix: *Acta Metall.*, 1987, vol. 35, pp. 1149–58.
40. R. Uemori, R. Chijiiwa, H. Tamehiro, and H. Morikawa: *Appl. Surf. Sci.*, 1994, vol. 76, pp. 255–60.
41. D.C. Houghton, G.C. Weatherly, and J.D. Embury: in *Thermomechanical Processing of Microalloyed Austenite*, A.J. DeArdo, G.A. Ratz, and P.J. Wray, eds., AIME, Pittsburg, 1982, pp. 267–92.
42. J.G. Speer, R.W. Regier, D.K. Matlock, and S.G. Jansto: in *Proceedings, New Developments on Metallurgy and Applications of High Strength Steels*, T. Perez, ed., Tenaris, Ternium, and Argentina Association of Materials, Buenos Aires, Argentina, 2008, p. 13.
43. C.M. Enloe, K.O. Findley, C.M. Parish, M.K. Miller, B.C. De Cooman, and J.G. Speer: *Scripta Mater.*, 2013, vol. 68, pp. 55–58.
44. W.B. Lee, S.G. Hong, C.G. Park, K.H. Kim, and S.H. Park: *Scripta Mater.*, 2000, vol. 43, pp. 319–24.
45. S. Kanazawa, A. Nakashima, K. Okamoto, K. Tanabe, and S. Nakazawa: *Trans. Jpn. Inst. Met.*, 1967, vol. 8, pp. 105–12.
46. S. Kanazawa, A. Nakashima, K. Okamoto, K. Tanabe, and S. Nakazawa: *Trans. Jpn. Inst. Met.*, 1967, vol. 8, pp. 113–20.
47. A. Ghosh, S. Das, and S. Chatterjee: *Mater. Sci. Technol.*, 2005, vol. 21, pp. 325–33.
48. S.Q. Yuan, G.L. Liang, and X.J. Zhang: *J. Iron. Steel Res. Int.*, 2010, vol. 17, pp. 60–63.
49. K. Tomita, Y. Funakawa, T. Shiozaki, E. Maeda, and T. Yamamoto: *Materia Japan*, 2003, vol. 42, pp. 70–72.
50. K. Seto, Y. Funukawa, and S. Kaneko: *JFE Technical Report*, 2007, pp. 19–25.
51. Y. Funakawa, T. Shiozaki, K. Tomita, T. Yamamoto, and E. Maeda: *ISIJ Int.*, 2004, vol. 44, pp. 1945–51.
52. I.B. Timokhina, P.D. Hodgson, S.P. Ringer, R.K. Zheng, and E.V. Pereloma: *Mater. Sci. Forum*, 2007, vols. 561–565, pp. 2083–86.
53. C.Y. Chen, H.W. Yen, F.H. Kao, W.C. Li, C.Y. Huang, J.R. Yang, and S.H. Wang: *Mater. Sci. Eng. A*, 2009, vol. 499, pp. 162–66.
54. J.H. Jang, C.H. Lee, Y.U. Heo, and D.W. Suh: *Acta Mater.*, 2012, vol. 60, pp. 208–17.
55. K. Nakagawa, T. Yokota, and K. Seto: in *Proceedings of the International Conference on New Developments in Advanced High-Strength Sheet Steels*, AIST, Orlando, 2008, pp. 209–18.
56. S.G. Davidson, J.P. Wise, and J.G. Speer: in *Proceedings of the 20th ASM Heat Treating Conference*, ASM International, St. Louis, 2000, pp. 1144–1151.
57. K. Narita: *Trans. ISIJ*, 1975, vol. 15, pp. 145–51.
58. L.M. Rothleutner, R. Cryderman, and C.J. Van Tyne: *Metall. Mater. Trans. A*, 2014, vol. 45A, pp. 4594–609.
59. F Kurosawa, I Taguchi, and R Matsumoto: *J. Jpn. Inst. Met. Mater.*, 1979, vol. 43, pp. 1068–77.
60. R.A. Grange, C.R. Hribal, and L.F. Porter: *Metall. Trans. A*, 1977, vol. 8A, pp. 1775–85.
61. G.R. Speich and W.C. Leslie: *Metall. Trans. A*, 1972, vol. 3A, pp. 1043–54.
62. K.J. Irvine and F.B. Pickering: *J. Iron Steel Inst.*, 1960, vol. 194, pp. 137–53.
63. N.C. Law and D.V. Edmonds: *Metall. Trans. A*, 1980, vol. 11A, pp. 33–46.
64. G.M. Michal and I.E. Locci: *Scr. Metall.*, 1988, vol. 22, pp. 1801–806.